Titre: Title:	Critical Evaluation and Thermodynamic Optimization of the Cu-Zn, Cu-Se and Zn-Se Binary Systems
Auteurs: Authors:	Yu Tang, Jie Ma, Dong Han, Jian Wang, Haiying Qi, & Liling Jin
Date:	2022
Type:	Article de revue / Article
Référence: Citation:	Tang, Y., Ma, J., Han, D., Wang, J., Qi, H., & Jin, L. (2022). Critical Evaluation and Thermodynamic Optimization of the Cu-Zn, Cu-Se and Zn-Se Binary Systems. Metals, 12(9), 1401 (32 pages). https://doi.org/10.3390/met12091401

Titre de la revue: Journal Title:	Metals (vol. 12, no. 9)
Maison d'édition: Publisher:	Multidisciplinary Digital Publishing Institute
URL officiel: Official URL:	https://doi.org/10.3390/met12091401
Mention légale: Legal notice:	© 2022 Tang, Y., Ma, J., Han, D., Wang, J., Qi, H., & Jin, L.. Licensee MDPI, Basel, Switzerland. This article is an open access article distributed under the terms and conditions of the Creative Commons Attribution (CC BY) license (https://creativecommons.org/licenses/by/ 4.0/).

metals

MDPI

Article

Critical Evaluation and Thermodynamic Optimization of the Cu-Zn, Cu-Se and Zn-Se Binary Systems

Yu Tang [1], Jie Ma [2,*], Dong Han [1], Jian Wang [1,3,*], Haiying Qi [4,*] and Liling Jin [5]

1 College of Mechanical Engineering, Yangzhou University, Yangzhou 225127, China
2 School of Materials and Chemical Engineering, Anhui Jianzhu University, Hefei 230601, China
3 Department of Materials Science and Engineering, Seoul National University, Seoul 151742, Korea
4 School of Materials Science and Hydrogen Energy, Foshan University, Foshan 528000, China
5 Center for Research in Computational Thermochemistry (CRCT), Department of Chemical Engineering, Ecole Polytechnique de Montréal, Montréal, QC H3C 3A7, Canada
* Correspondence: majie726@163.com (J.M.); Jian.wang@polymtl.ca (J.W.); haiyingqi@fosu.edu.cn (H.Q.)

Abstract: In our study, a complete review of the literature, critical evaluation and thermodynamic assessment of the Cu-Zn, Cu-Se and Zn-Se binary systems were carried out. The modified quasi-chemical model (MQM) was applied to describe the Gibbs energy of the liquid phase. The Gibbs energies of all intermetallic compounds and terminal solid solutions were described using the compound energy formalism (CEF) model. The re-optimization of the Cu-Zn binary system was carried out by considering the ordered bcc_B2 crystal structure of the β′ phase. Moreover, the β and δ phases in the Cu-Zn binary system with the same bcc_A2 crystal structure were modeled as one single phase in the present work. A self-consistent thermodynamic database was constructed for the Cu-Zn, Cu-Se and Zn-Se binary systems, work that formed part of a comprehensive thermodynamic database development project researching zinc-based biodegradable materials.

Keywords: thermodynamics; CALPHAD; Cu-Zn system; Cu-Se system; Zn-Se system

Citation: Tang, Y.; Ma, J.; Han, D.; Wang, J.; Qi, H.; Jin, L. Critical Evaluation and Thermodynamic Optimization of the Cu-Zn, Cu-Se and Zn-Se Binary Systems. *Metals* **2022**, *12*, 1401. https://doi.org/10.3390/met12091401

Academic Editor: Jiri Svoboda

Received: 23 June 2022
Accepted: 19 August 2022
Published: 24 August 2022

1. Introduction

Zinc-based alloys are a new kind of biodegradable material proposed by researchers. Zinc plays a vital role in the human body and is actively involved in constructing many mechanisms and functions, such as cell proliferation and bone metabolism [1]. Zinc-based alloys deserve to be regarded as a new exciting research field because of their moderate corrosion rate [2]. A review of zinc-based alloys has been conducted, focusing on the exploration of their cytotoxicity, biocompatibility, processing, corrosion rate and mechanical properties [3–7]. Recently, some new kinds of zinc-based alloys, such as porous zinc scaffolds, have been developed [8,9]. A new generation of Zn-Cu binary alloys have been investigated as biodegradable cardiovascular implant materials, which show good antibacterial properties against Staphylococcus aureus, with Cu concentrations greater than 2 wt.% according to in vitro experimental results [10]. Xiao et al. [11] provided a detailed description of Zn-Ag alloys as biodegradable materials and reviewed a series of advances in related research fields. Su et al. [12] concluded that zinc-based ceramic biomaterials are being developed as synergistic nanocomposite platforms that can combine cancer targeting, bio-imaging and responsive drug delivery with other potential applications. Jones et al. [13] evaluated the prospects of zinc-based applications in wound closure devices (e.g., absorbable sutures, staples, surgical staples, etc.). Yuan et al. [14] provided an outlook on the prospects of designing bio-functionalized coatings on the surface of zinc-based brain transfer materials. Since the degradation behavior of alloys in vivo affects their mechanical integrity and even their biocompatibility, and affects bioactivity directly through degradation products, Li et al. [15] conducted a study on the choice of extraction media and its effects on the cytotoxicity of zinc and its alloys.

However, the main problem with zinc-based is their lack of mechanical strength compared to iron-based and magnesium-based alloys, which limits the application of zinc-based alloys as implantable materials. Up to now, several series of zinc-based alloys, such as Zn-Mg-based, Zn-Cu-based, and Zn-Mn-based alloys, have been developed. Unfortunately, most zinc-based alloys were not afforded the mechanical properties matched to the human body and ideal biocompatibility. To enhance the mechanical properties of zinc-based alloys, many alloying elements, such as Ag, Ca, Sr, Se, Li, Y etc., were considered in order to improve the strength and toughness of Zn alloys [16–19].

Copper is a common additive element in Zn-based alloys, with a moderate solid solubility in the zinc matrix. The mechanical properties of Zn alloys can be improved by solution strengthening. Tang et al. [10] reported that adding Cu to zinc-based alloys could improve their tensile strength in research on cardiovascular scaffolds. In addition, the fracture elongation of Zn-based alloys can be improved by increasing their Cu content, which significantly meets the requirements for stent implantation. For example, Bednarczyk et al. [20] reported that the prepared Zn-0.5Cu alloy exhibited superplastic characteristics, and the elongation reached 510% using the ECAP treatment at room temperature. Niu et al. [21] reported that the grains of alloys could be refined clearly with the Cu additive.

Selenium, as one of the essential trace elements in the human body, participates in human metabolism, enhances human immunity, improves physical quality and delays the body aging. The proposed daily intake of selenium for the human body is 60–70 μg/d [22,23]. A lack of selenium will cause a decline in human immunity, increasing the incidence of tumors, cardiovascular diseases, liver diseases, and so on. Among its characteristics, the antioxidant properties of selenium protein play an important role in maintaining the cardiovascular system and skeletal muscles, which can effectively protect the cardiovascular system and repair muscle [24,25]. Selenium also has a protective effect on oxidative stress and anti-defense systems in the kidney, according to some experimental animal model test results [26–28]. Therefore, selenium can be regarded as a potential candidate additive element for the development of Zn-based medical materials. However, only a few studies have reported on the application of selenium in medical alloys as so far. Persaud-Sharma et al. [29] studied the application of Se to Mg-Zn-based alloys in cardiovascular stents. They pointed out that the elastic modulus of the alloy can be adapted to the cardiovascular system due to the addition of Se.

Although the secondary phase and solution strengthening are important for improving the properties of Zn-based alloys, information on the thermodynamic modeling phase equilibria of Zn-Cu-Se system has rarely been investigated. To design new Zn-Cu-Se alloys and investigate the relationship between their microstructure and mechanical properties, knowledge of the accurate phase equilibria in the Zn-Cu-Se systems is required. However, obtaining such results only through experiments is often complicated and expensive. Therefore, the best economic approach is to systematically obtain the thermodynamic properties of multi-component systems by the calculation of phase diagrams (CALPHAD) [30]. Our goal was to construct a thermodynamic database for calculating the phase equilibria of Zn-based multicomponent systems using the CALPHAD method. The modified quasi-chemical model (MQM) for the liquid phase was used, which can better describe the short-range ordered behavior in the liquid solution compared to the Bragg–Williams model (BMW) and associated model (AM) [31]. For the solid solutions, the compound energy formalism (CEF) was used to describe the Gibbs free energy functions, according to the sub-lattice structure [32].

In the present work, a complete literature review, critical evaluation and thermodynamic assessment of the Cu-Zn, Cu-Se, and Zn-Se binary systems were carried out using the CALPHAD approach [30]. This is a part work of our group's wider development project of a thermodynamic database for zinc-based multicomponent system, which could benefit the development of zinc-based biodegradable materials.

2. Critical Review of the Experimental Literature Data

2.1. Cu-Zn Binary System

There are many thermodynamic investigations on solid and liquid alloys of the Cu-Zn binary system. However, the experimental data is significantly scattered. The data on the phase equilibria and thermodynamic properties of Cu-Zn binary systems available in the literature were critically evaluated and re-optimized in the present work.

As early as 1904, a phase diagram of the Cu-Zn binary system was first reported by Shepherd [33]. Based on the previous experimental data [34–38], Hansen [39] evaluated the Cu-Zn phase diagram in 1936. The current accepted Cu-Zn phase diagram was established by Raynor [40]. Later, some minor modifications were suggested by Hansen and Anderko [41] and Massalski [42]. The last critical evaluation was performed by Miodownik [43]. Eight solution phases, liquid, fcc_A1, β (bcc_A2), β′ (bcc_B2), γ (Cu_5Zn_8), δ (bcc_A2), hcp_A3 and hcp_Zn, were confirmed in the Cu-Zn binary system. However, there were still some uncertainties concerning the phase boundaries below the temperature of about 400 °C.

There are already several thermodynamic descriptions of the Cu-Zn binary system in the literature [44–50]. Spencer [44] published the first one in 1986. Later, Kowalski and Spencer [45] carried out a better thermodynamic evaluation, fitting well with the experimentally assessed phase diagram except for the Zn-rich corner [43]. This thermodynamic description was accepted in the COST507 (COST531) database [51]. To facilitate the description of ternary Al-Cu-Zn systems, Liang and Chang [46] simplified the description of the γ (Cu_5Zn_8) phase from a four-sub-lattice to a single sub-lattice model. Based on the COST507 database [52], David et al. [47] modified the thermodynamic description, adopting their own electromotive force (EMF) measurements of Zn-rich alloys. Gierlotka and Chen [48] provided two sets of thermodynamic descriptions by considering or disregarding the β (bcc_A2)/β′ (bcc_B2) disorder–order transition. However, the ordered β′ (bcc_B2) phase and disordered β (bcc_A2) phase were treated as two separated phases. They also introduced the concept of temperature dependence for the enthalpy during the mixing of the liquid phase based only on the derived experimental enthalpy data, which was not reasonable. To combine it with the γ (Cu_5Zn_8) phase in Al-Cu system, Wang et al. [49] changed the model of the γ (Cu_5Zn_8) phase to be $(Zn)_4(Cu, Zn)_1(Cu, Zn)_8$ based on the COST507 database [51], which was modeled as $(Al)_4(Al, Cu)_1(Cu)_8$. The model of $(Al)_4(Al, Cu)_1(Cu)_8$ for the γ (Cu_5Zn_8) phase in the Al-Cu system was only used to constrain the composition range of the γ (Cu_5Zn_8) phase and did not consider any information on the crystal structure. Similar to Wang et al. [49], Liang et al. [50] re-optimized the Cu-Zn system to build a comprehensive thermodynamic description of the ternary Al-Cu-Zn system. In their paper, the four-sub-lattice model for the γ(Cu_5Zn_8) phase was simplified to be $(Cu)_4(Cu, Zn)_6(Cu, Zn)_{16}$, without considering its realistic crystal structure. In addition, the δ phase was modeled as a separate phase by Liang et al. [50], which was modeled as the same phase, BCC_A2, in the previous assessment [44–46,48,49].

In summary, after carefully evaluating all the previous thermodynamic descriptions, we found that none of the thermodynamic descriptions of the Cu-Zn binary system could be directly extrapolated to multi-component systems because of the inconsistent models, which prevents the construction of databases of multicomponent systems for the purpose of high-throughput computational material design.

The crystal structure of the cubic γ phase in the Cu_5Zn_8 prototype structure is a highly complex one, which stabilizes over a relatively wide composition range. The unit cell contains 52 atoms occupying four sets of sites denoted by 8c, 8c, 12e and 24g (Wyckoff notation). The distribution of the Cu and Zn atoms over all the sites was investigated by Bradley et al. [52] using the XRD technique in 1931, Heidenstam et al. [53] using neutron diffraction in 1968 and Gourdon et al. [54] using neutron and XRD diffraction in 2007. Mixing Cu and Zn on all four sub-lattices, eliminated by Heidenstam et al. [53], fostered a rather poor agreement with the diffraction data. Thus, the evidence for the atomic distribution of Cu and Zn is not conclusive. The mixing of Cu and Zn at site 8c has been

accepted by Kowalski and Spencer [45]. Based on the experimental results of Gourdon et al. [54], Cu and Zn atoms prefer to substitute at the M3 (12e) and M4 (24g) sites. In this paper, the model $(Cu)_2(Zn)_2(Cu, Zn)_3(Cu, Zn)_6$ was used to describe the γ (Cu_5Zn_8) phase based on the crystal structure and atomic distribution information.

The crystal structure of the δ (bcc_A2) phase was first investigated by Schubert and Wall [55], who reported it as cubic structure. Later, Lenz and Schubert [56] corrected this description, adding that the δ (bcc_A2) phase is hexagonal. Degtyareva [57] confirmed that the formation of the hexagonal structure of the δ (bcc_A2) phase is the structural distortion of the body-centered cubic lattice. Thus, the δ phase and the β phase should be modeled the same as the phase bcc_A2.

All the original experimental works on the thermodynamic properties of Cu-Zn binary systems were examined carefully and collected in Table 1. All the directly measured data were used in the present work for the thermodynamic optimization instead of the derived data. A typical case of derived data is that regarding integral enthalpy, obtained from experiments on the temperature dependence of the experimental vapor pressure, or EMF data. These direct data are compiled in Table 1.

The enthalpies of the mixing of liquid Cu-Zn alloys, ΔH_m^{liquid}, at 1127 °C [58] and 1100 °C [59] were directly measured by the calorimetry method. The results obtained by Parameswaran [58] when $x_{Zn} > 0.5$ showed a large deviation. Samson-Himmelstjema [60] calculated the liquid properties at 1000 °C based on their measured enthalpy values of the solid phases at 20 °C. There were significant discrepancies between the different results.

The relative chemical potentials of Zn in liquid Cu-Zn alloys, μ_{Zn}^{liquid}, were determined by Schneider and Schmid [61] (700–850 °C), Everett et al. [62] (796–1030 °C), Downie [63] (927 °C), Azakami and Yazawa [64] (850–1200 °C), Solov'ev et al. [65] (1100 °C) and Sugino and Hawara [66] (1050–1150 °C) using a variety of vapor pressure methods; by Leitgebel [67] (915–1500 °C) and Baker [68] (1150 °C) using the boiling point method; and by Kleppa and Thalmayer [69] (627 °C) and Gerling and Predel [70] (800–900 °C), adopting the EMF measurement method. The vapor pressure technique was used at temperatures ranging from 700 to 1200 °C, the boiling point method was used from 915 to 1500 °C, and the EMF investigation was conducted at temperatures ranging from 627 to 900 °C. In general, the results of these different experiments were in strong agreement.

The enthalpies of the formation of the solid fcc_A1 phases were measured by calorimetric investigations by Samson-Himmelstjerna [60] (20 °C), Körber and Oelsen [71] (25 °C), Weibke [72] (90 °C), Kleppa and King [73] (25 °C), Orr and Argent [74] (300 °C) and Blair and Downie [75] (300–400 °C). The enthalpies of the formation of the β′ (bcc_B2), γ (Cu_5Zn_8) and hcp_A3 phases were measured by the calorimetry method as well [60,71,72,75]. Because it is challenging to attain equilibrium in the specimens used for calorimetric measurements at room temperature, the experimental data on the homogeneity range were doubtful for the ordered β′ (bcc_B2) phase and γ (Cu_5Zn_8) phase.

The chemical potentials of Zn in the solid phase in the Cu-Zn system have been intensively studied by the referenced studies [76–81]. The experimental data on the chemical potentials of Zn in the solid fcc_A1 phase were in agreement with each other at lower Zn concentrations (less than 0.1 at. % Zn), which increasingly diminished with increasing Zn concentrations. The results on the chemical potentials of Zn in the β (bcc_A2) phase determined by Ölander [76] contradicted the values obtained by Seith and Krauss [77] and Hargreaves [78], which showed considerable differences. The available results for γ (Cu_5Zn_8) and hcp_A3 phases were only obtained by Ölander [76].

Table 1. Summary of original experimental results [58–81] on the thermodynamic properties of the Cu-Zn binary system.

Properties	Experimental Method	Temperature Range (°C)	Composition Range (at% Zn)	Refs.
ΔH_m^{liquid}	Calorimetry	1127	5–85	[58]
	Adiabatic calorimeter	1100	10–40	[59]
	Calorimetry	1000	0–100	[60]
μ_{Zn}^{liquid}	Vapor pressure technique	700–850	42.8–79.8	[61]
	Vapor pressure technique	796–1030	32.9–79.2	[62]
	Vapor pressure technique	927	8.1–85.3	[63]
	Vapor pressure technique	850–1200	5–92	[64]
	Vapor pressure technique	1100	1–10	[65]
	Vapor pressure technique	1100–1150	1–8	[66]
	Boiling point method	915–1500	6.5–88.55	[67]
	Boiling point method	1150	18–90	[68]
	EMF	627	80–92	[69]
	EMF	800–900	20–90	[70]
ΔH_f^{solid}	Calorimetry	20	12–88	[60]
	Calorimetry	25	11.2–87.8	[71]
	Calorimetry	90	39–98	[72]
	Calorimetry	25	7–37	[73]
	Calorimetry	300	10–35	[74]
	Calorimetry	300–400	26–86.5	[75]
μ_{Zn}^{solid}	Vapor pressure technique	850	20–60	[76]
	EMF	400, 500	44.4–84.3	[77]
	Vapor pressure technique	727	37.3–45.3	[78]
	Vapor pressure technique	727	2.1–34.1	[79]
	Atomic absorp-tionmethod	500	5–35	[80]
	Vapor pressure technique	790	1–10	[81]

2.2. Cu-Se Binary System

The Cu-rich part of the Cu-Se phase diagram was reviewed by Hansen and Anderko [41] based on previous experimental data. Later, Heyding [82], Bernardini et al. [83], Murray and Heyding [84], Babitsyna et al. [85], Glazov and Kim [86] and Glazov et al. [87] re-investigated the phase diagram of the Cu-Se system in restricted composition ranges. Glazov et al. [88]

assessed the phase equilibria of the Cu-Se system accordingly. The liquid phase exhibited two miscibility gaps in the Cu-rich region above 1100 °C [85] and in the Se-rich region above 523 °C [84], respectively. The boundary for the high-temperature miscibility gap at the copper-rich region was determined by [86], which suggested a high critical temperature. The highest temperature area of the liquidus line, in the vicinity of Cu_2Se, was determined by Glazov et al. [87] (32.5–35.6 at. % Se) using the high-precision differential thermal analysis (DTA) method. The liquid miscibility gap in the Se-rich region is characterized by a high Se vapor pressure. Thus, there is only one data point (98. 2 at. % Se, 963 °C) on the Se-rich side [89]. The fcc_A1 terminal solid solution of Cu exhibited negligible solubility of Se, and the rhombohedral terminal solid solution of Se exhibited negligible solubility of Cu. Seven stable phases were reported in the Cu-Se system: β-$Cu_{2-x}Se$, α-Cu_2Se, Cu_3Se_2, α-CuSe, β-CuSe, γ-CuSe and $CuSe_2$. The lower temperature phase of α-Cu_2Se was reported to be stable below 123 °C, with a relatively narrow homogeneity range [84]. All the compounds in the Cu-Se system, except the β-$Cu_{2-x}Se$ phase, were stoichiometric, with a negligible homogeneity range. The high-temperature β-$Cu_{2-x}Se$ was stable between 123 ± 15 °C and 1130 °C, at stoichiometry (x = 0), with a broad homogeneity range extending on the Se side to form a defect compound. The homogeneity range of β-$Cu_{2-x}Se$ at room temperature was reviewed by Chakrabarti and Laughlin [90]. The reported range was approximately between 35.4 and 36.0 at. % Se, corresponding to $0.18 \leq x \leq 0.22$ in the β-$Cu_{2-x}Se$ phase. The homogeneity range increased further at higher temperatures. Muhsin [91] measured the homogeneity range of β-$Cu_{2-x}Se$ at 627 °C, Δx = 0.012, which was less than the previous measurement value, Δx = 0.106 at 652 °C, reported by Bernardini [83].

Gattow and Schneidener [92], Askerova et al. [93] and Rau and Rabenau [94] measured the enthalpies of the formation of the compounds α-Cu_2Se, β-$Cu_{2-x}Se$, α-CuSe, Cu_3Se_2 and $CuSe_2$ at 298.15 K by the calorimetry method, the EMF method and vapor pressure method. Mills et al. [95] evaluated the data based on the previous experimental results. For β-$Cu_{2-x}Se$, the enthalpies of formation were estimated in by [94]. Their results were a little scattered, whereas the data evaluated by Mills et al. [95] were reasonable to some extent. The standard entropies of the compounds $CuSe_2$, CuSe, Cu_3Se_2 and Cu_2Se at 298.15K were reported by Askerova et al. [93], Rau and Rabenau [94] and Mills [95] as well.

Stølen et al. [96] measured the heat capacity of α-CuSe, β-CuSe and γ-CuSe by the adiabatic shield calorimetry method from T = 5 K to 653 K. Heat capacity data for α-Cu_2Se and β-Cu_2Se were reported by Kubaschewski and Nolting [97] and Blachnik and Gunia [98]. The heat capacity value at 300 K reported by Blachnik and Gunia [98] was too large, and we have doubts about its validity. The heat of the fusion of Cu_2Se was measured by Murray and Heyding [84] and Glazov and Mendelevich [99]. The heat of the γ-CuSe peritectic decomposition and the transformation heat for α-CuSe/β-CuSe were determined by Stølen et al. [96].

For the liquid phase, the activities of Cu and Se at 1100 °C were determined by Blachnik and Bolte [100]. Askerova and Yazawa [101] calculated the activities of Cu and Se at 1200 °C and 1150 °C by the Gibbs–Duhem integration. These were difficult to illustrate in the figure because of their very small value. The original experimental results of the thermodynamic properties of the different Cu-Se compounds are presented in Table 2.

Du et al. [102] optimized the Cu-Se system using the associate model for the liquid phase. The calculated heat capacities of Cu_2Se were not in strong agreement with the experimental data [97,98]. Moreover, the β-$Cu_{2-x}Se$ phase was stable from a high temperature to room temperature. However, in [102], it was only stable above 378 K. Thus, the Cu-Se binary system was re-optimized in the present work.

Table 2. Summary of the original experimental work [84,93–100] on the thermodynamic properties of the Cu-Se system at 298.15 K.

Phases	$\Delta_f H^0_m$ (kJ·mol^{-1})	S^0_m (J·K^{-1}·mol^{-1})	$C^0_{p,m}$ (J·K^{-1}·mol^{-1})	Experimental Method	Temperature (K)	Refs.
A-CuSe	−(39.5 ± 0.5)			calorimetry		[92]
	−(33.5 ± 10.0)	74.1		EMF		[93]
	−40.6	72.0		Vapor pressure		[94]
	−41.8	78.2		Evaluation		[95]
		(79.3 ± 0.8)	(50.3 ± 0.6)	adiabatic calorimetry	5–653 K	[96]
β-CuSe	$\Delta_{trans}H^0_m$ = 0.8553		heat capacity	adiabatic calorimetry	5–653 K	[96]
γ-CuSe	$\Delta_{dec}H^0_m$ = 11.8		heat capacity	adiabatic calorimetry	5–653 K	[96]
α-Cu_2Se	−(59.3 ± 0.5)			calorimetry		[92]
	−(65.7 ± 6.5)	80.2		EMF	320 to 420 K	[93]
	−65.3	157.3		Vapor pressure		[94]
	−65.3	129.7		Evaluation		[95]
			heat capacity		180 to 560 K	[97]
			75.23 (300K)	drop calorimetry	350 to 1500 K	[98]
β-Cu_2Se	−(54.4 ± 0.5)			calorimetry		[92]
	−57.5(Cu1.75Se)	162.3		Estimation		[94]
	−54.0(Cu1.75Se)			Evaluation		[95]
	$\Delta_{trans}H^0_m$ = (6.4 ± 2.0)			Evaluation		[84]
	$\Delta_{trans}H^0_m$ = (6.5 ± 2.0)			Evaluation		[99]
$CuSe_2$	−(43.1 ± 4)			calorimetry		[92]
	−(39.3 ± 4)	98.4		EMF		[93]
	−48.1	120.5		Vapor pressure		[94]
	−48.1	107.5		Vapor pressure		[95]
Cu_3Se_2	−(98.9 ± 7.1)			calorimetry		[92]
	−(94.6 ± 7.1)	184.9		EMF		[93]
	−104.6	207.1		EMF		[94]

2.3. Zn-Se Binary System

The Zn-Se system was reviewed by Sharma and Chang [101] and Brebrick and Liu [103]. Only one intermediate phase, ZnSe, was reported in the Zn-Se binary system, which is congruently formed. There are three different polymorphs: α-ZnSe, with the zinc blende (sphalerite) structure, which is stable to the melting point; β-ZnSe, with the sodium chloride structure being is stable only at high pressures; and the third form of ZnSe, with the wurtzite structure that is metastable at all temperatures and pressures. However, Okada et al. [104] indicated that α-ZnSe transformed to the wurtzite-type structure at 1411 °C, according to their DTA results.

The melting point of ZnSe was measured at 1515 ± 20 °C by Fischer [105], at 1526 ± 10 °C by Sysoev et al. [106] and at 1522 ± 2 °C by Okada et al. [104]. Sharma and Chang [107] assessed the temperature to be 1526 °C. In the present work, the melting point of ZnSe was taken to be 1522 °C. Since the values of Fischer [105] and Sysoev et al. [106] were obtained under high pressure inert gas conditions, the T_m may be affected by the deviation from the congruent composition due to the dissociative evaporation of ZnSe.

The liquidus data of the whole Zn-Se binary system have been less rigorously studied. It was determined by [108–111] only over the range of 0–9 at.% Se, and 68–90 at.% Se and 99–100 at.% Se by [112,113]. The liquid miscibility gap and the monotectic reaction in the

Zn-ZnSe region were predicted by Sharma and Chang [101] and compared to the similar liquid miscibility gap in the Zn-Te system [114]. In the present study, both the experimental results and calculated results by Sharma and Chang [101] were considered.

The mutual solid solubilities of Zn and Se have not been measured, which are most likely negligible. The crystal structures of the solid phases in the Zn-Se system are listed in Table 3. The standard enthalpies and entropies of the formation of α-ZnSe at 298.15 K were reported by Korneeva et al. [115], Wösten et al. [116], Sedgwick [117], Terpilowski et al. [118], Flögel [119], Hassan et al. [120], Kirk et al. [121], Bardi et al. [122], Nasar et al. [123], Brebrick and Liu [103] and Schönherr et al. [124]. The original experimental data are all summarized in Table 3. The average standard enthalpies and entropies of formation were calculated giving equal weight to these results, excepting those in [115], which are marked by a star symbol. Chen et al. [125] optimized the Zn-Se system using the associate solution model for the liquid phase. In this study, the Zn-Se system was re-optimized using the MQM model for the liquid phase. The ZnSe phase was treated as a stoichiometric phase in the present work.

Table 3. Summary of the original experimental work [103,115–125] on the standard entropy of the α-ZnSe phase at 298.15 K.

ΔH_m^0 (kJ·mol^{-1})	S_m^0 (J·K^{-1}·mol^{-1})	Experimental Method	Temperature (K)	Refs.
−(215.9 ± 35.0)	(31.6 ± 20.0)	Knudsen effusion weight loss	913–1093	[115]
−(198.6 ± 19.0)	(58.9 ± 14.0)	Gas flow method	1060–1393	[116]
−(185.8 ± 16.0)	(62.2 ± 20.0)	Static method	900–1200	[117]
−(166.1 ± 6.0)	(69.9 ± 6.0)	Electrochemical cell	360–420	[118]
−(192.5 ± 23.0)	(54.9 ± 12.0)	Gas flow method	1173–1413	[119]
−(157.8 ± 13.0)	(88.7 ± 12.0)	Knudsen torsion effusion	952–1209	[120]
−(164.5 ± 6.0)	(86.2 ± 9.0)	Mass spectrometry and Knudsen effusion weight loss	923–1123	[121]
−(183.4 ± 14.0)	(66.1 ± 9.0)	Knudsen effusion weight loss	1025–1288	[122]
−(177.5 ± 6.0)	(59.4 ± 12.0)	Electrochemical cell	635–693	[123]
−(175.0 ± 6.0)	(63.9 ± 9.0)	Electrochemical cell	693–825	[123]
−(177.1 ± 8.0)			707	[123]
−(175.4 ± 8.0)	(74.0 ± 6.0)	Optical density	1260–1410	[103]
−(182.4 ± 14.0)	(68.1 ± 14.0)	Knudsen effusion weight loss	1190–1310	[124]
−175.9	13.2	Calculated		[125]
−163.85	11.8	Calculated		This work

3. Thermodynamic Modeling

The optimizations of the Cu-Zn, Cu-Se and Zn-Se binary systems were carried out with the Factsage thermodynamic software [126]. The thermodynamic parameters of the pure elements were extracted from the SGTE database [127]. All phases and their thermodynamic models involved in these binary systems are listed in Table 4.

Table 4. Structural parameters of the phases and thermodynamic models used in the present work.

Phase	Pearson Symbol	Strukturbericht Designation	Space Group	Prototype	Refs.	Model
Liquid						MQM
α-Cu (fcc_A1)	cF4	A1	$Fm\bar{3}m$	Cu	[43]	CEF
β (bcc_A2)	cI2	A2	$Im\bar{3}m$	W	[48]	CEF
β′ (bcc_B2)	cP2	B2	$Pm\bar{3}m$	CsCl	[48]	CEF
γ (Cu_5Zn_8)	cI52	D82	$I\bar{4}3m$	Cu_5Zn_8	[51]	CEF
δ (bcc_A2)	cI2	A2	$Im\bar{3}m$	W	[55]	CEF
ε (hcp_A3)	hP6	A3	$P6_3/mmc$	Mg	[43]	CEF
η (hcp_Zn)	hP2	A3	$P6_3/mmc$	Mg	[43]	CEF
hex_A8	hP3	A8	$P3_121$	hexagonal_A8	[43]	CEF
β-$Cu_{2-x}Se$			$Fm\bar{3}m$	fcc	[83]	CEF
α-Cu_2Se			$P12_1/c1$	monoclinic	[88]	ST
Cu_3Se_2			$P\bar{4}2_1m$	hexagonal	[88]	ST
α-CuSe			$P6_3/mmc$	hexagonal	[88]	ST
β-CuSe			Cmcm	hexagonal	[88]	ST
γ-CuSe			$P6_3/mmc$	orthorhombic	[88]	ST
$CuSe_2$			Pnnm	orthorhombic	[88]	ST
ZnSe	hP4	B4	$P6_3mc$	ZnS (wurtzite)	[103]	ST

MQM: modified quasi-chemical model, CEF: compound energy formalism, ST: stoichiometric compound.

3.1. Liquid Phase

The thermodynamic properties of the liquid phase were modeled with the MQM model developed by Pelton et al. [128,129]. The associated notation and detailed description of the MQM model are given in [128,129]. The same notations are used in the present work, and a brief description of MQM model is given as follows:

Taking the Cu-Zn binary system, for example, the quasi-chemical pair exchange reaction can be considered:

$$(\mathrm{Cu}-\mathrm{Cu})_{pair}+(\mathrm{Zn}-\mathrm{Zn})_{pair}=2(\mathrm{Cu}-\mathrm{Zn})_{pair},\Delta g_{\mathrm{CuZn}} \quad (1)$$

where the Cu-Zn pair represents a first-nearest-neighbor pair of atoms. The Gibbs energy change of the formation of one mole of the Cu-Zn pairs with Cu-Cu and the Zn-Zn pairs is $\frac{\Delta g_{\mathrm{CuZn}}}{2}$. Let n_{Cu} and n_{Zn} be the number of moles of Cu and Zn, according to Reaction (1). n_{CuCu}, n_{ZnZn}, and n_{CuZn} be the number of moles of the Cu-Cu, Zn-Zn and Cu-Zn pairs. Z_{Cu} and Z_{Zn} are the coordination numbers of Cu and Zn. Then, the Gibbs energy of the solution is given by:

$$G=\left(n_{\mathrm{Cu}}G^0_{\mathrm{Cu}}+n_{\mathrm{Zn}}G^0_{\mathrm{Zn}}\right)-T\Delta S^{config}+\left(\frac{n_{\mathrm{CuZn}}}{2}\right)\Delta g_{\mathrm{CuZn}} \quad (2)$$

where G^0_{Cu} and G^0_{Zn} are the molar Gibbs energies of the pure components Cu and Zn, and ΔS^{config} is the configurational entropy of the mixing, given by randomly distributing the Cu-Cu, Zn-Zn and Cu-Zn pairs in the one-dimensional Ising approximation. The expression for ΔS^{config} is as follows:

$$\Delta S^{config} = -R(n_{\mathrm{Cu}} ln X_{\mathrm{Cu}} + n_{\mathrm{Zn}} ln X_{\mathrm{Zn}}) - R\left(n_{\mathrm{CuCu}} ln \frac{X_{\mathrm{CuCu}}}{Y_{\mathrm{Cu}}^2} + n_{\mathrm{ZnZn}} ln \frac{X_{\mathrm{ZnZn}}}{Y_{\mathrm{Zn}}^2} + n_{\mathrm{CuZn}} ln \frac{X_{\mathrm{CuZn}}}{Y_{\mathrm{Cu}} Y_{\mathrm{Zn}}}\right) \quad (3)$$

where X_{CuCu}, X_{ZnZn} and X_{CuZn} are the mole fractions of the Cu-Cu, Zn-Zn and Cu-Zn pairs, respectively. Y_{Cu} and Y_{Zn} are the coordination-equivalent fractions of Cu and Zn, which can be expressed as:

$$X_{ij} = \frac{n_{ij}}{n_{AA} + n_{BB} + n_{AB}} (i,\ j = \mathrm{Cu}\ or\ \mathrm{Zn}), \quad (4)$$

$$X_i = \frac{Z_i n_i}{Z_A n_A + Z_B n_B} (i = \mathrm{Cu}\ or\ \mathrm{Zn}) \quad (5)$$

Moreover, the following elemental balance equations can be written as follows:

$$Z_{\mathrm{Cu}} n_{\mathrm{Cu}} = 2n_{\mathrm{CuCu}} + n_{\mathrm{CuZn}}, \quad (6)$$

$$Z_{\mathrm{Zn}} n_{\mathrm{Zn}} = 2n_{\mathrm{ZnZn}} + n_{\mathrm{CuZn}}, \quad (7)$$

It may be noted that there is no exact expression for the configurational entropy in three dimensions. Although Equation (3) is only an approximate expression in three dimensions, it is exact one dimensionally (when Z = 2) [128]. As explained in [128], one is forced by the approximate nature of Equation (3) to use non-exact values for the coordination numbers in order to yield a good fit between the experimental data and the calculated ones. The mathematical approximation of the one-dimensional Ising model of Equation (3) can be partially compensated by selecting values of Z_{Cu} and Z_{Zn} which are smaller than the experimental values [130]. As is known, the MQM model is sensitive to the ratio of the coordination numbers, but less sensitive to their absolute values. From a practical standpoint, for developing large thermodynamic databases, the values of Z_{Cu} and Z_{Zn} of the order of 6 have been deemed necessary for solutions with a small or medium degree of ordering (i.e., alloy solutions).

The item Δg_{CuZn} is the model parameter for reproducing the excess Gibbs energy of the Cu-Zn liquid phase, which can be expressed as follows:

$$\Delta g_{\mathrm{CuZn}} = \Delta g^0_{\mathrm{CuZn}} + \sum_{i \geq 1} g^{s0}_{\mathrm{CuZn}} (X_{\mathrm{CuCu}})^s + \sum_{j \geq 1} g^{0t}_{\mathrm{CuZn}} (X_{\mathrm{ZnZn}})^t \quad (8)$$

where g^0_{CuZn}, g^{s0}_{CuZn} and g^{0t}_{CuZn} are the adjustable model parameters, which can be functioned according to the temperature dependence. The s and t are exponential powers, which can be set to 0, 1, 2, and so on. The equilibrium state of the system is obtained by minimizing the total Gibbs energy at a constant elemental composition, temperature and pressure. The equilibrium pair distribution is calculated by setting:

$$\left(\frac{\partial G}{\partial n_{\mathrm{CuZn}}}\right) n_{\mathrm{Cu}} n_{\mathrm{Zn}} = 0, \quad (9)$$

This gives the "equilibrium constant" for the "quasi-chemical pair reaction" of Equation (10):

$$\frac{X^2_{\mathrm{CuZn}}}{X_{\mathrm{CuCu}} X_{\mathrm{ZnZn}}} = 4 \times \exp\left(-\frac{\Delta g_{\mathrm{CuZn}}}{RT}\right), \quad (10)$$

Moreover, the model permits Z_{Cu} and Z_{Zn} to vary, with the composition as follows [128]:

$$\frac{1}{Z_{\mathrm{Cu}}} = \frac{1}{Z^{\mathrm{Cu}}_{\mathrm{CuCu}}} \left(\frac{2n_{\mathrm{CuCu}}}{2n_{\mathrm{CuCu}} + n_{\mathrm{CuZn}}}\right) + \frac{1}{Z^{\mathrm{Cu}}_{\mathrm{CuZn}}} \left(\frac{n_{\mathrm{CuZn}}}{2n_{\mathrm{CuCu}} + n_{\mathrm{CuZn}}}\right) \quad (11)$$

$$\frac{1}{Z_{Zn}} = \frac{1}{Z^{Zn}_{ZnZn}}\left(\frac{2n_{ZnZn}}{2n_{ZnZn}+n_{CuZn}}\right) + \frac{1}{Z^{Zn}_{CuZn}}\left(\frac{n_{CuZn}}{2n_{ZnZn}+n_{CuZn}}\right) \quad (12)$$

where Z^{Cu}_{CuCu} and Z^{Zn}_{CuZn} are the values of Z_{Cu} when all the nearest neighbors of a Cu atom are Cu atoms, and when all nearest neighbors of a Cu atom are Zn atoms, respectively. Z^{Zn}_{ZnZn} and Z^{Zn}_{CuZn} are defined similarly. The composition of the maximum short-range ordering (SRO) is determined by the ratio of the coordination numbers $Z^{Cu}_{CuZn}/Z^{Zn}_{CuZn}$. The values of the coordination numbers chosen in the present study are listed in Table 5.

Table 5. The present optimized parameters of the liquid phase in the Cu-Zn, Cu-Se and Zn-Se systems.

Coordination Numbers *				Gibbs Energies of the Pair Exchange Reactions (J/mol-atoms)
m	***n***	Z^m_{mn}	Z^n_{mn}	
Cu	Zn	6	6	$\Delta g_{Cu,Zn} = -8300.0 + 0.89 \times T - (3000.0 - 1.30 \times T)X_{CuCu} + (2450.0 - 3.44 \times T)X_{ZnZn} - 1000.0X^4_{ZnZn}$
Cu	Se	7.5	4	$\Delta g_{Cu,Se} = -23600.0 - 4.30 \times T + (42900.0 - 8.63 \times T)X_{CuCu} - 13000.0X^2_{CuCu} + 15000.0X_{SeSe} + (17000.0 - 4.80 \times T)X^4_{SeSe}$
Zn	Se	4	4	$\Delta g_{Zn,Se} = -66398.5 + 1.14 \times T - (36999.9 - 2.09 \times T)X_{ZnZn} - 8999.7X^2_{ZnZn} + 25982.6X_{SeSe} - 12999.6X^2_{SeSe}$

* For all pure elements (Cu, Zn, Se), $Z^m_{mm} = Z^n_{nn} = 6$

3.2. Solution Phases

In the present work, the solid phases hcp_Zn, hex_A8, bcc_A2 and fcc_A1 were modeled with the single sub-lattice as (Zn, Cu, Se). The configuration entropy of the Bragg–Williams-type and a sub-regular solution approximations was used for the excess Gibbs energy and the configurational entropy of the Bragg–Williams type. Hillert et al. [32] introduced the CEF model to describe the solid phase Gibbs energy with the sub-lattice, and an ideal mixing on each sub-lattice was assumed. The intermetallic compounds of the binary systems were modeled by using sub-lattice models based on the crystal structure and solid solutions. The definition of the Gibbs energy depended on the appropriate choice of lattice stoichiometry and the mixture of substances in any given lattice.

Taking the β-$Cu_{2-x}Se$ phase as an example, and the Gibbs energy expression of β-$Cu_{2-x}Se$ phase, based on the CEF model, which is obtained by mixing the Cu and Se elements on two sub-lattices with a stoichiometric ratio of 2:1 as $(Cu, Se)_2(Cu, Se)$, the Gibbs energy can be expressed as follows:

$$\begin{aligned} G^{Cu_2Se} = {} & y^I_{Cu}y^{II}_{Se}G^0_{Cu:Se} + y^I_{Cu}y^{II}_{Cu}G^0_{Cu:Cu} + y^I_{Se}y^{II}_{Se}G^0_{Se:Se} + y^I_{Se}y^{II}_{Cu}G^0_{Se:Cu} + RT\left(y^I_{Cu}\ln y^I_{Cu} + y^I_{Se}\ln y^I_{Se}\right) \\ & + 2RT\left(y^{II}_{Cu}\ln y^{II}_{Cu} + y^{II}_{Se}\ln y^{II}_{Se}\right) + y^I_{Cu}y^{II}_{Cu}y^{II}_{Se}{}^nL_{Cu:Cu,Se} + y^I_{Se}y^{II}_{Cu}y^{II}_{Se}{}^nL_{Se:Cu,Se} \\ & + y^I_{Cu}y^I_{Se}y^{II}_{Se}{}^nL_{Cu,Se:Se} + y^I_{Cu}y^I_{Se}y^{II}_{Cu}{}^nL_{Cu,Se:Cu} \end{aligned} \quad (13)$$

The y^I_{Cu}, y^I_{Se}, y^{II}_{Cu} and y^{II}_{Se} here represent the positional fractions of Cu and Se on the first and second sub-lattices, respectively. $y^0_{Cu:Se}$, $y^0_{Cu:Cu}$, $y^0_{Se:Se}$, and $y^0_{Se:Cu}$ are the Gibbs energy of terminal members, respectively. ${}^nL_{i:i:j}$ represents the interaction energy between Cu and Se on the second sub-lattice when the first sub-lattice is taken up by Cu or Se, and ${}^nL_{i:j:i}$ represents the interaction energy between Cu and Se on the first sub-lattice when the second sub-lattice is taken up by Cu or Se.

The sub-lattice formalism applied to the bcc_A2 and bcc_B2 phases was introduced by Dupin and Ansara [131], and the same notations were used in the present work. The Gibbs energy functions of the bcc_A2 and bcc_B2 phases were modeled as one single bcc phase with the combined sub-lattice structures as one single sub-lattice (Cu, Zn) for the disorder part (bcc_A2), and two sub-lattices (Cu, Zn)(Cu, Zn) for the ordered part (bcc_B2). The molar Gibbs energy of the whole bcc phase with these disordered (bcc_A2) and ordered (bcc_B2) parts can be expressed as follows:

$$G^{bcc} = G^{disorder}_{bcc\_A2} + G^{order}_{bcc\_B2} \quad (14)$$

where $G_{bcc\_A2}^{disorder}$ is the Gibbs energy contribution of the bcc phase from the disordered part (bcc_A2), modeled with a signgle sublattice (Cu, Zn). The Gibbs energy expression of bcc_A2 can be written as follows:

$$G_{bcc\_A2}^{disorder} = x_{\mathrm{Cu}}{}^{0}G_{\mathrm{Cu}}^{bcc\_A2} + x_{\mathrm{Zn}}{}^{0}G_{\mathrm{Zn}}^{bcc\_A2} + RT(x_{\mathrm{Cu}}\ln x_{\mathrm{Cu}} + x_{\mathrm{Zn}}\ln x_{\mathrm{Zn}}) + x_{\mathrm{Cu}}x_{\mathrm{Zn}}\sum_{n=0}^{2}(x_{\mathrm{Cu}} - x_{\mathrm{Zn}})^{n\,n}L_{\mathrm{Cu,Zn}}^{disorder} \quad (15)$$

The items ${}^{0}G_{\mathrm{Cu}}^{bcc\_A2}$ and ${}^{0}G_{\mathrm{Zn}}^{bcc\_A2}$ are the Gibbs energy of the pure Cu and Zn with a bcc_A2 crystal structure. ${}^{n}L_{i,j}^{disorder}$ refers to the interaction parameters of the disordered part of the bcc phase (bcc_A2).

In the equation below, $G_{bcc\_B2}^{order}$ is the Gibbs energy contribution of the bcc phase from the ordered part (bcc_B2), modeled with two sublattices (Cu, Zn)(Cu, Zn). The Gibbs energy of bcc_B2 can be expressed as follows:

$$\begin{aligned} G_{bcc_{B2}}^{order} = \sum_{i,j=Cu,\ Zn} & y_i^{\mathrm{I}}y_j^{\Pi 0}G_{i:j}^{bcc_{B2}} + RT\left(y_i^{\mathrm{I}}\ln y_i^{\mathrm{I}} + y_j^{\mathrm{I}}\ln y_j^{\mathrm{I}} + \ldots\right) + RT\left(y_i^{\Pi}\ln y_i^{\Pi} + y_j^{\Pi}\ln y_j^{\Pi} + \ldots\right) \\ & + y_i^{\mathrm{I}}y_j^{\mathrm{I}}\sum_{n=0}^{2}\left(y_i^{\mathrm{I}} - y_j^{\mathrm{I}}\right)^{n}{}^{n}L_{i,j:i}^{\mathrm{I}} + y_i^{\Pi}y_j^{\Pi}\sum_{n=0}^{2}\left(y_i^{\Pi} - y_j^{\Pi}\right)^{n}{}^{n}L_{i,j:i}^{\Pi} \end{aligned} \quad (16)$$

where ${}^{0}L_{i,j}^{bcc\_B2}$ is the Gibbs energy of the hypothetical compound ij: CuZn, CuCu, ZnCu and ZnZn. Items ${}^{n}L_{i,j:i}^{\mathrm{I}}$ and ${}^{n}L_{i:i,j}^{\Pi}$ are the interaction parameters of the ordered part of bcc_B2. Due to the crystallographic symmetry of the bcc_B2 phase, the following relations are introduced:

$${}^{0}G_{i:j}^{bcc\_B2} = {}^{0}G_{j:i}^{bcc\_B2};\ {}^{0}L_{i,j:i}^{\mathrm{I}} = {}^{0}L_{i:i,j}^{\Pi} \quad (17)$$

Moreover, relations exist in the parameters between the ordered and disordered solutions, which were used in the present work and were described in detail in [131].

3.3. Stoichiometric Intermetallic Compounds

In the present work, the seven intermetallic compounds α-Cu_2Se, Cu_3Se_2, α-CuSe, β-CuSe, γ-CuSe, $CuSe_2$ and ZnSe were treated as stoichiometric compounds. The Gibbs energy per mole of the formula unit Cu_xSe_y is expressed as follows:

$$G_x^{\mathrm{Cu_xSe_y}} = xG_{\mathrm{Cu}}^{\mathrm{fcc\_A1}} + yG_{\mathrm{Se}}^{\mathrm{hex\_A8}} + \Delta G_f^{\mathrm{Cu_xSe_y}} \quad (18)$$

where $\Delta G_f^{\mathrm{Cu_xSe_y}}$ is the Gibbs energy of the formation per mole of the formula unit Cu_xSe_y.

Because of the sufficiency of the heat capacity data for the compound CuSe [40], the ΔC_p of CuSe is given by the formula:

$$\Delta C_p = a + b \times T + c/T + d \times T^2 + e/T^3 + f/T^{10} \quad (19)$$

where the parameters a, b, c, d, e and f were evaluated in the present work.

The molar Gibbs energies of the pure elements and stoichiometric phases can be described by:

$$G_T^0 = H_T^0 - TS_T^0, \quad (20)$$

$$H_T^0 = \Delta^{298.15K}H_f^0 + \int_{298.15K}^{T} C_p dT, \quad (21)$$

$$S_T^0 = \Delta^{298.15K}S_f^0 + \int_{298.15K}^{T} (C_p/T)dT, \quad (22)$$

where $\Delta^{298.15K}H_f^0$ is the molar enthalpy of the given substance generated by the pure element ($\Delta^{298.15K}H_f^0$ of the stable element was determined as 0 J·mol at T = 298.15 K and the pressure of 101.3kPa, as the reference state), $\Delta^{298.15K}H_f^0$ is the molar entropy at T = 298.15 K and C_p is the molar heat capacity. The heat capacity of alloys in the Zn-Se and Cu-Se binary

systems, which were evaluated by the Neumann-Kopp rule [132], were not reported in the experiment.

4. Results and Discussion

4.1. Cu-Zn Binary System

The present calculated phase diagram of the Cu-Zn system, compared with the original experimental data from Bauer and Hansen [36], Ruer and Kremers [37] and Parameswaran and Healy [58], is shown in Figure 1. Based on previous experimental results [36], Ruer and Kremers [37] re-investigated the Cu-Zn system using the thermal analysis method. The liquidus data provided by Parameswaran and Healy [58] using the calorimetry method showed a slight difference with [37], especially in the Zn-rich region. Miodownik [43] critically reviewed the experimental phase diagram of the Cu-Zn binary system, omitting the EMF results provided by David et al. [47]. Figure 1 represents the calculated phase diagram in this work together with the results of [43]. The calculated liquidus curve, located between the illustrations of [37] and [58], fit well with the invariant reaction temperatures of the assessed phase diagram [43], as shown in Figure 1. In addition, the limited thermodynamic information for the boundaries of these phases, fcc_A1, β′ (bcc_B2), γ (Cu_5Zn_8) and hcp_A3, at the temperature below about 400 °C, illustrated by Hansen and Anderko [41], represented an uncertainty. This is because the present broad-scale optimization work resulted in minor differences from the previously calculated results [45,50].

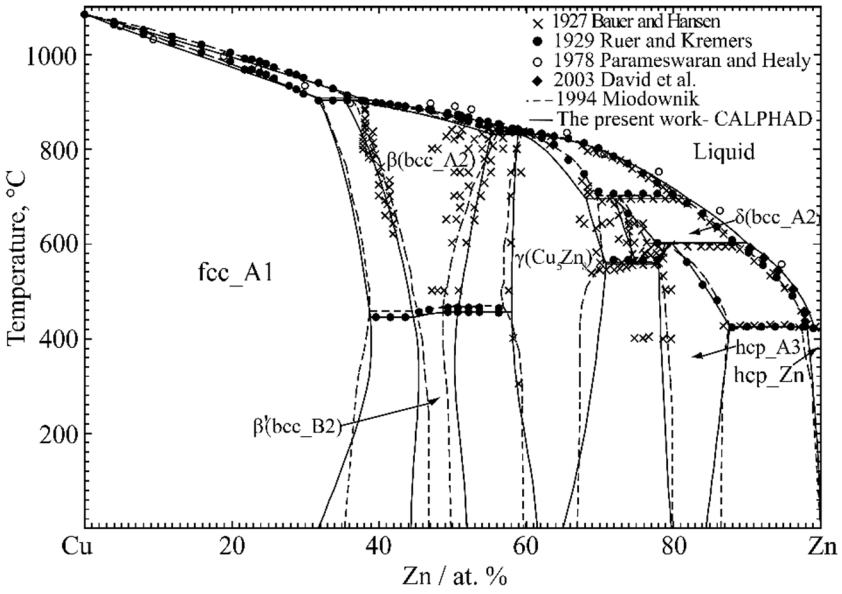

Figure 1. The calculated phase diagram of the Cu-Zn system compared with the experimental data from refs. [36,37,43,58].

The present calculated phase diagram, compared with the previous optimized results by Spencer [44] and Liang et al. [50], is shown in Figure 2. The thermodynamic description by Spencer [44] agreed well with the experimentally assessed phase diagram [43], excepting the Zn-rich corner. In the present study, the liquid solution was modeled by the MQM model, and the seven solid solutions were modeled by the CEF model. All the parameters of the thermodynamic models obtained in this work are listed in Tables 5 and 6. A complete comparison of the present work with the previous thermodynamic descriptions [45,47,48,50] and the experimentally assessed basis [43] is provided for the invariant reactions in Table 7. Compared with the experimental data [43], the present calculated phase diagram and invariant reactions show an improvement in the liquidus curve and Zn-rich corner compared with the work of [45], while maintaining the same level of agreement in the rest of the phase diagram. Moreover, Liang et al. [50] determined the γ (Cu_5Zn_8) phase to be $(Cu)_4(Cu,$

$Zn)_6(Cu, Zn)_{16}$, without considering information about the detailed crystal structure. In addition, the δ phase should not be modeled as a separate phase, which has the same bcc_A2 crystal structure as the bcc solution phase. Gierlotka and Chen [48] provided two sets of thermodynamic descriptions by considering or disregarding the β (bcc_A2)/β′ (bcc_B2) disorder–order transition. However, the ordered β′ (bcc_B2) phase and disordered β (bcc_A2) phase were modeled as two separated phases. The ordered β′ phase should be modeled as the ordered part (bcc_B2) of the bcc phase, as discussed above. Therefore, the phases of δ, β and β′, were treated as one single bcc phase. Then, they were modeled with the two parts of the Gibbs energy functions, with (Cu, Zn) for the disordered bcc_A2 part and (Cu, Zn)(Cu, Zn) for the ordered bcc_B2 part. As shown in Figure 1, the present optimized results of the bcc phase are in strong agreement with the available experimental data. Moreover, thanks to the more reliable experimental data in the composition region of 90–98 at. % Zn reported David et al. [47], the modeling of liquidus in the Zn-rich region was improved in the present work. Compared with the original experimental data [36,37,47,58] and previously optimized results [45,47,50], the presently calculated results show a reasonable agreement with the experimental results and other calculated results.

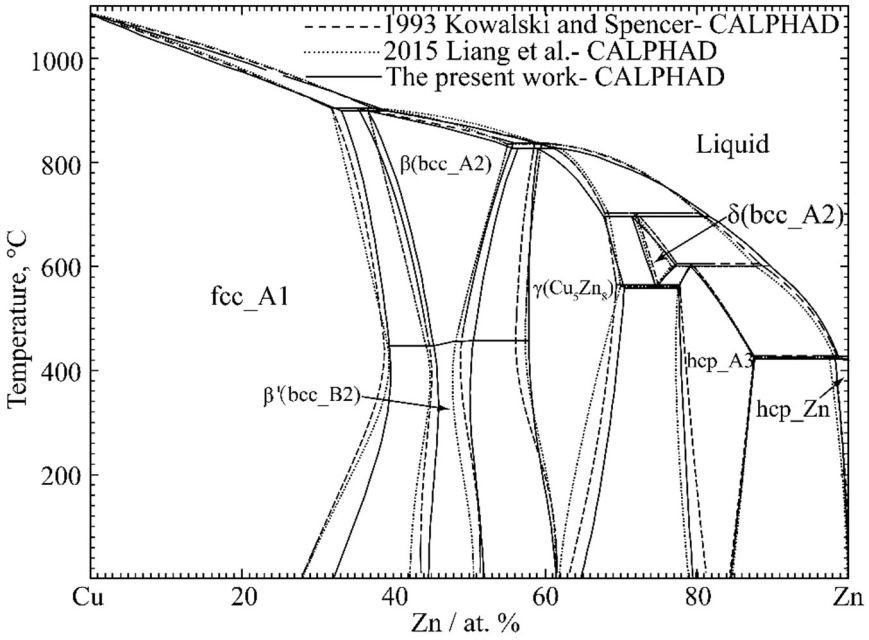

Figure 2. The calculated phase diagram of the Cu-Zn system compared with the previously optimized data from refs. [45,50].

Table 6. Optimized thermodynamic parameters of the solid solutions and compounds in the Cu-Zn, Cu-Se and Zn-Se binary systems.

Phase, Model and Thermodynamic Parameters (J/mol, or J/(mol·K))	Refs.
Fcc_A1 phase, format (Cu, Zn, Se):	
$G_{Cu} = {}^{0}G_{Cu}^{fcc\_A1}$; $G_{Zn} = {}^{0}G_{Zn}^{hcp\_Zn} + 2969.8 + 1.57 \times T$; $G_{Se} = {}^{0}G_{Se}^{hex\_A8} + 20920.0$;	[127]
${}^{0}L_{Cu,Zn} = -42804.0 + 10.02 \times T$; ${}^{1}L_{Cu,Zn} = 2936.0 - 3.05 \times T$; ${}^{2}L_{Cu,Zn} = 9034.0 - 5.39 \times T$;	This work
${}^{0}L_{Cu,Se} = 70000.0$;	This work
Bcc_A2 phase, format (Cu, Zn):	
$G_{Cu} = {}^{0}G_{Cu}^{fcc\_A1} + 4017.0 + 1.26 \times T$; $G_{Zn} = {}^{0}G_{Zn}^{hcp\_Zn} + 2887.0 + 2.51 \times T$;	[127]
${}^{0}L_{Cu,Zn} = -51460.0 + 13.06 \times T$; ${}^{1}L_{Cu,Zn} = 7862.0 - 6.45 \times T$; ${}^{2}L_{Cu,Zn} = 30400.0 - 29.92 \times T$;	This work
β'(bcc_B2) phase, format $(Cu, Zn)_{0.5}(Cu, Zn)_{0.5}$:	
$G_{Cu:Cu}^{ord,B2} = G_{Zn:Zn}^{ord,B2} = 0$; $G_{Cu:Zn}^{ord,B2} = G_{Zn:Cu}^{ord,B2} = -9180.0 + 4.25 \times T$;	This work
Hcp_A3 phase, format (Cu, Zn):	
$G_{Cu} = {}^{0}G_{Cu}^{fcc\_A1} + 600.0 - 0.20 \times T$; $G_{Zn} = {}^{0}G_{Zn}^{hcp\_Zn} + 2969.8 + 1.57 \times T$;	[127]
${}^{0}L_{Cu,Zn} = -36845.0 + 5.79 \times T$; ${}^{1}L_{Cu,Zn} = 25277.0 - 9.55 \times T$;	This work
Hcp_Zn phase, format (Cu, Zn):	
$G_{Zn} = {}^{0}G_{Zn}^{hcp\_Zn}$; $G_{Cu} = {}^{0}G_{Cu}^{fcc\_A1} + 600.0 - 0.20 \times T$;	[127]
${}^{0}L_{Cu,Zn} = -14432.0 - 10.78 \times T$;	This work
γ (Cu_5Zn_8) phase, format $(Cu)_2(Zn)_2(Cu, Zn)_3(Cu, Zn)_6$:	
$G_{Cu:Zn:Cu:Cu} = 11 \times G_{Cu}^{bcc\_A2} + 2 \times G_{Zn}^{bcc\_A2}$; $G_{Cu:Zn:Zn:Cu} = 8 \times G_{Cu}^{bcc\_A2} + 5 \times G_{Zn}^{bcc\_A2} + 250000.0$;	This work
$G_{Cu:Zn:Cu:Zn} = 5 \times G_{Cu}^{bcc\_A2} + 8 \times G_{Zn}^{bcc\_A2} - 184500.0 + 4.70 \times T$;	This work
$G_{Cu:Zn:Zn:Zn} = 2 \times G_{Cu}^{bcc\_A2} + 11 \times G_{Zn}^{bcc\_A2} - 89000.0 + 5.80 \times T$;	This work
Hex_A8 phase, format (Cu, Se):	
$G_{Cu} = {}^{0}G_{Cu}^{fcc\_A1} + 12552.0$; $G_{Se} = {}^{0}G_{Se}^{hex\_A8}$; ${}^{0}L_{Cu,Se} = 500.0$;	[127]
β-Cu_2Se phase, format $(Cu, Va)_2(Se)$:	
$G_{Cu:Se} = {}^{\beta-Cu_2Se}G^{*}_{\beta-Cu_2Se} - 70760.0 + 125.09 \times T$; $G_{Se} = {}^{0}G_{Se}^{hex\_A8} - 2092.0 - 46.02 \times T$;	This work
${}^{0}L_{Cu,Va:Se} = 11700.0 + 5.00 \times T$; ${}^{1}L_{Cu,Va:Se} = -41500.0 + 13.50 \times T$;	This work
α-Cu_2Se phase, format $(Cu)_2(Se)$:	
$G_{\alpha-Cu_2Se} = {}^{\alpha-Cu_2Se}G^{*}_{\alpha-Cu_2Se} - 75443.0 + 113.20 \times T$;	This work
γ-CuSe phase, format $(Cu)(Se)$: $G_{\gamma-CuSe} = {}^{\gamma-CuSe}G^{*}_{\gamma-CuSe} - 39540.0 + 6.26 \times T$;	This work
β-CuSe phase, format $(Cu)(Se)$: $G_{\beta-CuSe} = {}^{\beta-CuSe}G^{*}_{\beta-CuSe} - 800.0$;	This work
α-CuSe phase, format $(Cu)(Se)$: $G_{\alpha-CuSe} = {}^{\alpha-CuSe}G^{*}_{\alpha-CuSe} - 100.0$;	This work
Cu_3Se_2 phase, format $(Cu)_3(Se)_2$:	
$G_{Cu_3Se_2} = 3 \times {}^{0}G_{Cu}^{fcc\_A1} + 2 \times {}^{0}G_{Se}^{hex\_A8} - 112258.0 + 22.47 \times T$;	This work
$CuSe_2$ phase, format $(Cu)(Se)_2$: $G_{CuSe_2} = {}^{0}G_{Cu}^{fcc\_A1} + 2 \times {}^{0}G_{Se}^{hex\_A8} - 44610.0 + 0.35 \times T$;	This work
ZnSe phase, format $(Zn)(Se)$: $G_{ZnSe} = {}^{0}G_{Zn}^{hcp\_Zn} + {}^{0}G_{Se}^{hex\_A8} - 163850.0 - 11.80 \times T$;	This work
${}^{\beta-Cu_2Se}C_p = 398.7 - 0.9939 \times T + \frac{2108400}{T^2} + 0.0012348 \times T^2 - \frac{45150}{T} - \frac{3.543E7}{T^3}$ $298.15K \leq T \leq 413K$	This work
$= 82.41 + \frac{1.6545E27}{T^{10}}$ $413K \leq T \leq 3200K$;	
${}^{\alpha-Cu_2Se}G^{*}_{\alpha-Cu_2Se} = \int {}^{\alpha-Cu_2Se}C_p dt - T \times \int ({}^{\alpha-Cu_2Se}C_p/T) dt$;	This work
${}^{\alpha-Cu_2Se}C_p = 398.7 - 0.9939 \times T + \frac{2108400}{T^2} + 0.0012348 \times T^2 - \frac{45150}{T} - \frac{3.543E7}{T^3}$ $298.15K \leq T \leq 396K$;	This work
${}^{\gamma-CuSe}G^{*}_{\gamma-CuSe} = \int {}^{\gamma-CuSe}C_p dt - T \times \int ({}^{\gamma-CuSe}C_p/T) dt$;	

Figure 3 shows the calculated enthalpy of the mixing of the liquid phase at 900 and 1100 °C, together with the experimental data [58–61,63,68,70] and previously optimized results [45,48,50]. It should be noted that, among all the experimental data, only three sets [58–60] were directly measured by the calorimetry method. The other reported values of the enthalpy of the mixing data were derived from the measured vapor pressure and EMF results, which were converted into the chemical potential. Gierlotka and Chen [48] optimized the liquid phase based on the derived data of the enthalpy of the mixing, which presented as relatively high, as shown in Figure 3. The calculated enthalpy in the present work was in strong agreement with the experimental data by Samson-Himmelstjema [60]. In addition, the direct experimental data [58,59] are scattered. This may be due to the vapor pressures of the zinc being too high to affect the accuracy of the experimental results. The calculated results in the present work showed reasonable agreement with the experimental data in the Zn-poor region.

Table 7. The calculated invariant reactions in the Cu-Zn system compared with the experimental data from ref. [44] and calculated data from refs. [45,47,48,50].

Reaction	Reaction Type	Temperature (°C)	Composition (Zn at. %)			Refs.
Liquid + fcc_A1 ↔ β(bcc_A2)	Peritectic	903	36.8	31.9	36.1	[43]
		903	37.3	31.9	35.3	[32]
		902	37.2	31.9	35.1	[45]
		900			35.8	[48]
		902	36.7	31.9	36.0	[50]
		898	39.0	33.1	36.6	This work
Liquid + β(bcc_A2) ↔ γ(Cu_5Zn_8)	Peritectic	835	59.1	55.8	59.1	[43]
		835	59.2	55.8	58.6	[45]
		837	60.6	57.2	59.9	[47]
		834			58.7	[48]
		833	59.6	55.1	59.6	[50]
		824	61.8	56.3	59.1	This work
Liquid + γ(Cu_5Zn_8) ↔ δ(bcc_A2)	Peritectic	700	80.0	69.2	72.4	[43]
		700	80.2	67.8	71.9	[45]
		700	82.0	68.9	72.5	[47]
		703			72.0	[48]
		700	80.3	68.4	71.8	[50]
		695	81.7	67.7	71.7	This work
Liquid + δ(bcc_A2) ↔ hcp_A3	Peritectic	598	88.0	76.0	78.1	[43]
		600	88.2	77.3	79.2	[45]
		599	89.2	77.3	79.5	[47]
		600			79.2	[28]
		598	87.8	76.7	79.2	[50]
		602	89.6	77.2	79.2	This work
δ(bcc_A2) ↔ γ(Cu_5Zn_8) + hcp_A3	Eutectoid	560	74.0	70.0	78.0	[43]
		559	74.9	69.3	77.7	[45]
		560	74.3	69.0	77.6	[47]
		559	74.9			[48]
		560	74.6	70.0	77.6	[50]
		557	74.6	70.4	77.5	This work
Liquid + hcp_A3 ↔ hcp_Zn	Peritectic	424	98.3	87.2	97.2	[43]
		422	98.3	87.5	98.1	[45]
		419	98.4	87.4	97.6	[47]
		421			98.3	[48]
		425	98.2	87.5	97.3	[50]
		422	98.7	87.6	98.2	This work
β(bcc_A2) ↔ β′(bcc_B2) + (Cu_5Zn_8)	Ordering reaction	470	48.2	57.0		[43]
		469	49.1	56.1		[45]
		466	48.4	57.5		[50]
β(bcc_A2) ↔ β′(bcc_B2) + (Cu_5Zn_8)	Ordering reaction	456	50.5	57.8		This work
β(bcc_A2) ↔ β′(bcc_B2) + fcc_A1	Ordering reaction	453	44.8	38.3	72.4	[43]
		460	44.5	38.6	71.9	[45]
		456	44.2	39.2	77.5	[50]
		447	45.3	39.4		This work

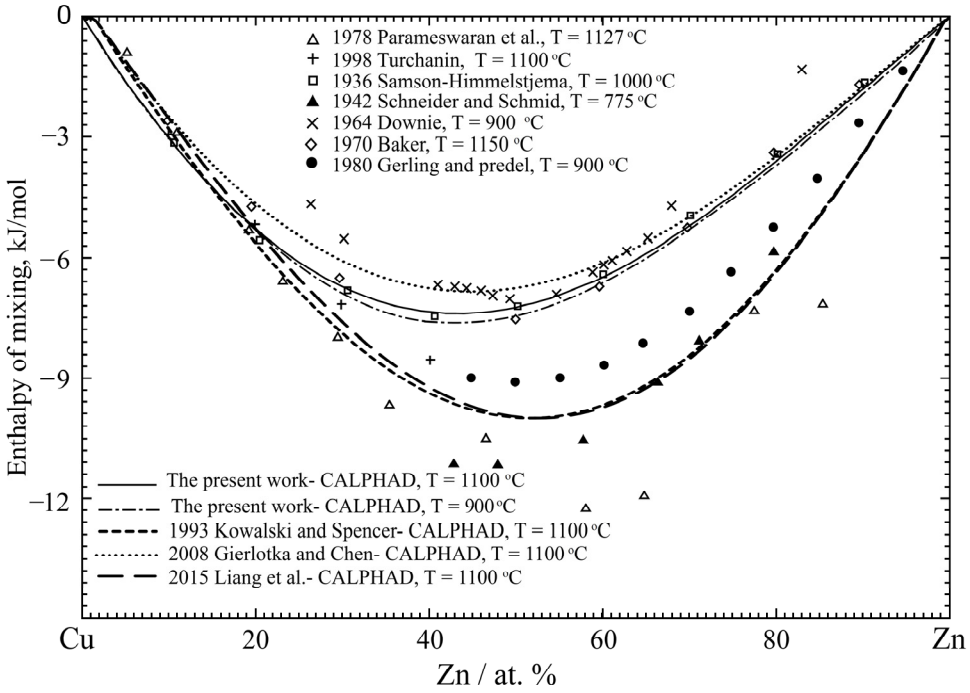

Figure 3. The calculated enthalpy of the mixing of the liquid phase at 900 and 1100 °C in the Cu-Zn system compared with the experimental data from refs. [58–61,63,68,70] and previously optimized calculations data from refs. [45,48,50].

The present calculated values of the relative chemical potential of Zn in the liquid phase at 627, 927, 1100 and 1200 °C reproduced the experimental results [61–70] very closely, as shown in Figure 4. The relative chemical potential of Zn in the liquid was calculated at different temperatures to compare the different experimental results, which varied only a little in the wide temperature range from 627 °C to 1200 °C.

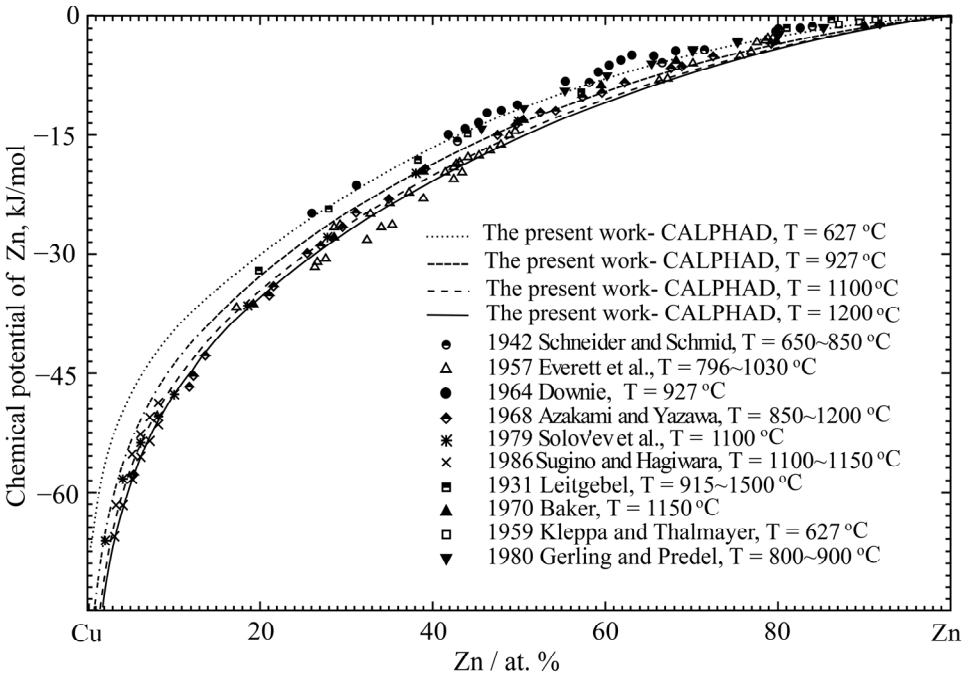

Figure 4. The calculated chemical potential of Zn for the liquid phase at 627, 927, 1100 and 1200 °C in the Cu-Zn system compared with the experimental data [61–70].

Figure 5 shows the calculated enthalpies of the formation of the solid phases at 25 °C and 300 °C, compared with the experimental data [60,71–75]. The present calculated results agree well with the experimental data. The formation enthalpy of the ordered β′ (Bcc_B2) phase shows a strong temperature dependence. The presently calculated chemical potential of Zn for the solid phases at 500 °C and 727 °C agrees with the experimental data [76–81], as shown in Figure 6. The experimental data for the fcc_A1 phase was scattered. The presently calculated chemical potential of Zn in the β (bcc_A2) and γ (Cu5Zn8) phases at 500 °C are in excellent accordance with the experimental data of Ölander [76].

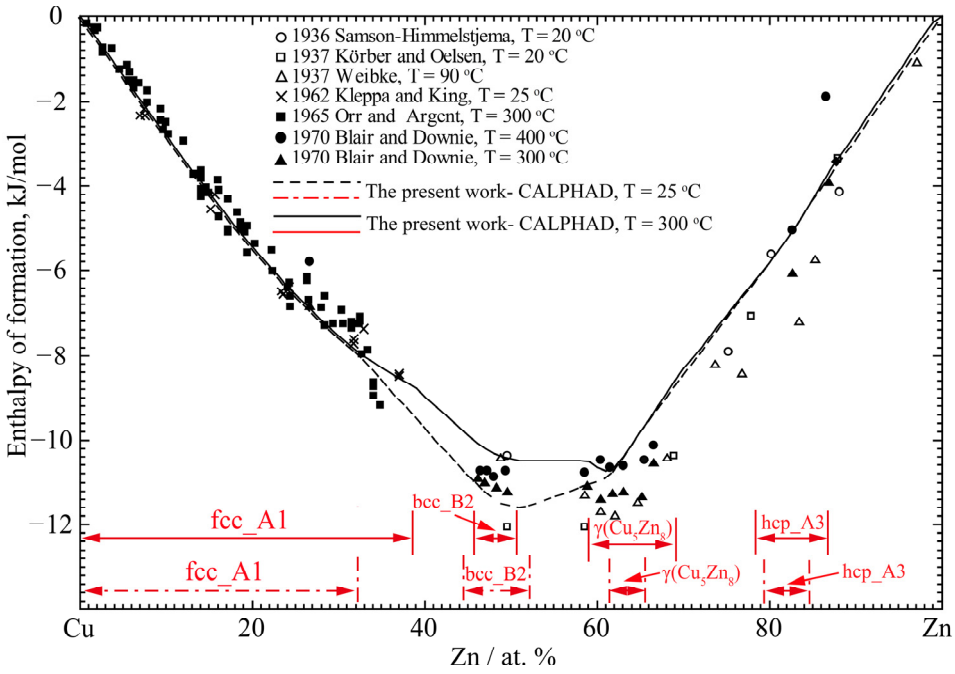

Figure 5. The calculated standard enthalpies of formation at 25 and 300 °C in the Cu-Zn system compared with the experimental data from refs. [60,71–75].

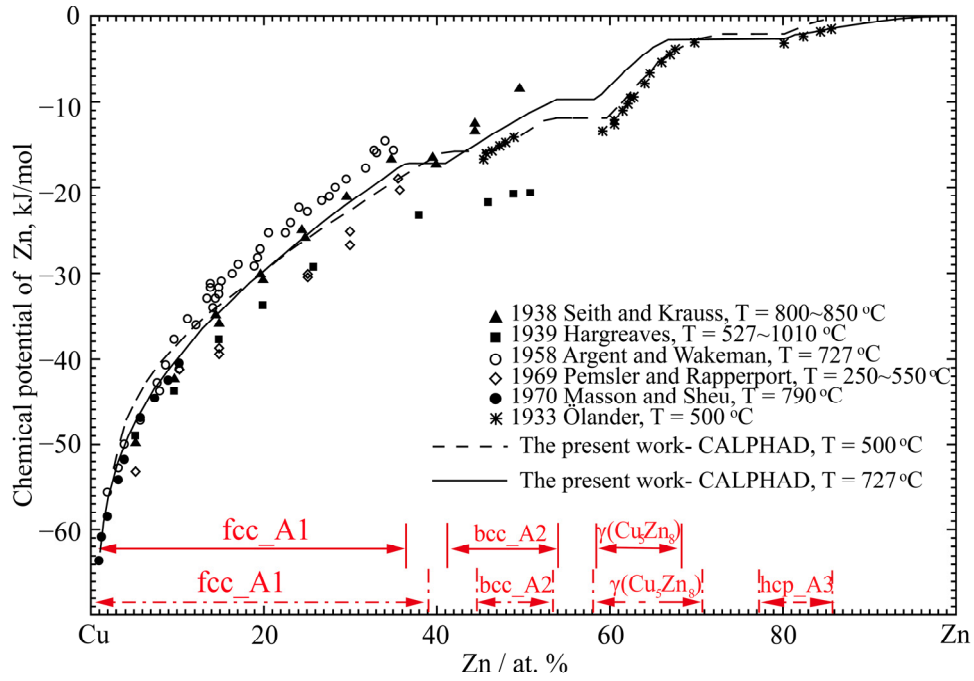

Figure 6. The calculated chemical potential of Zn for the solid phases at 500 and 727 °C in the Cu-Zn system compared with the experimental data from refs. [76–81].

4.2. Cu-Se Binary System

The optimized parameters of the stable phases in the Cu-Se binary system are listed in Tables 5 and 6. The phase equilibria and thermodynamic properties of this system were calculated using the optimized parameters, performed using the Factsage software.

The calculated phase diagram, compared with the experimental data [82–87] and the optimized results by Du et al. [102], is shown in Figure 7. The present calculated phase diagram agrees well with the available data. The calculated homogeneity range of β-$Cu_{2-x}Se$ at 627 °C, Δx = 0.028, is consistent with the results by Muhsin [91]. The presently calculated boundaries for the liquid miscibility gap at the Cu-end and the Se-end are in agreement with the experimental results [87,89]. The calculated invariant reactions, together with the experimental results and optimized results by Du et al. [100], are all listed in Table 8. As demonstrated in Table 8, the Cu-Se binary system was well reproduced in the present work.

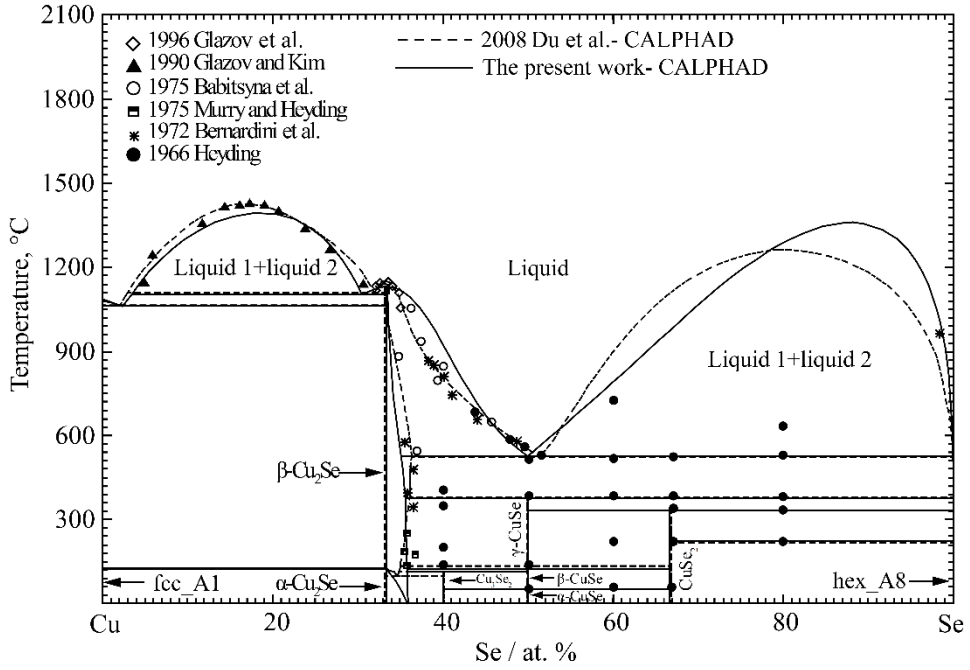

Figure 7. The calculated phase diagram of the Cu-Se system compared with the experimental data from refs. [82–87] and previously optimized results by Du et al. [102].

Figure 8 shows the standard enthalpy of formation in the Cu-Se system at 25 °C compared with the experimental data [92–95]. The presently optimized results are closer to the experimental data than that of Du et al. [100]. The standard entropy of formation at 25 °C, compared with the experimental data [92–95] and previously optimized results by Du et al. [100], is shown in Figure 9. Compared with the calculated results by Du et al. [100], the results of the present work show better agreement with the experimental data. As shown in Figures 10 and 11, the calculated enthalpy and entropy of mixing at 1127 °C, compared with the calculated results by Du et al. [100], indicate that our calculated results using the MQM model [128,129] are considerably more acceptable.

Table 8. The calculated invariant reactions in the Cu-Se system compared with the experimental data from ref. [88] and calculated data from ref. [100].

Reaction	Reaction Type	Temperature (°C)	Composition (Zn at. %)			Refs.
Liquid#1 + fcc_A1 ↔ β-Cu2Se	Eutectic	1063	1.8	0.0	33.3	[88]
		1062	2.1	0.0	33.3	[100]
		1060	2.3	0.0	33.3	This work
Liquid#2 ↔ liquid#1 + β-Cu2Se	Monotectic	1107			35.8	[48]
		1107	36.7	31.9	36.0	[50]
		1101	39.0	33.1	36.6	This work
Liquid#2 ↔ β-Cu2Se + liquid	Monotectic	523	52.5	36.5	99.6	[88]
		523	51.6	36.3	99.9	[100]
		525	50.0	35.1	99.9	This work
β-Cu2Se + liquid ↔ γ-CuSe	Peritectic	380	36.5	100.0	50.0	[88]
		380	36.1	100.0	50.0	[100]
		376	35.6	100.0	50.0	This work
β-Cu2Se + β-CuSe ↔ Cu3Se2	Peritectoid	112	36.3	50.0	40.0	[88]
		113	35.0	50.0	40.0	[100]
		113	35.8	50.0	40.0	This work
γ-CuSe + liquid ↔ $CuSe_2$	Peritectic	332	50.0	100.0	66.7	[88]
		332	50.0	100.0	66.7	[100]
		333	50.0	100.0	66.7	This work
Liquid ↔ CuSe2 + hex_A8	Peritectoid	221	~100	66.7	100.0	[88]
		221	~100	66.7	100.0	[100]
		221	~100	66.7	100.0	This work
Fcc_A1 + β-Cu2Se ↔ α-Cu2Se	Eutectoid	123	0.0	33.3	33.3	[88]
		123	0.0	33.3	33.3	[100]
		123	0.0	33.3	33.3	This work
Liquid ↔ β-Cu2Se	Congruent melting	1130	33.4	33.4		[88]
		1148	33.3	33.3		[100]
		1130	33.3	33.3		This work
γ-CuSe ↔ β-CuSe	Allotropic	120	50.0	50.0		[88]
		137	50.0	50.0		[100]
		120	50.0	50.0		This work
β(bcc_A2) ↔ β′(bcc_B2) + fcc_A1	Ordering reaction	54	50.0	50.0		[88]
		54	50.0	50.0		[100]
		51	50.0	50.0		This work

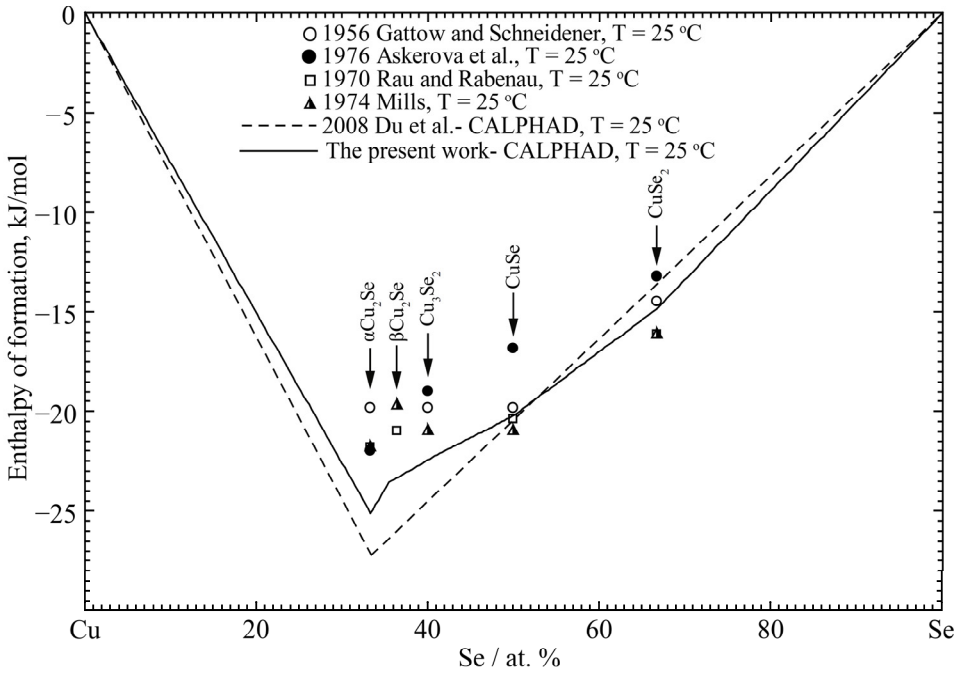

Figure 8. The calculated standard enthalpy of formation at 25 °C in the Cu-Se system compared with the experimental data from refs. [92–95] and previously optimized results by Du et al. [100].

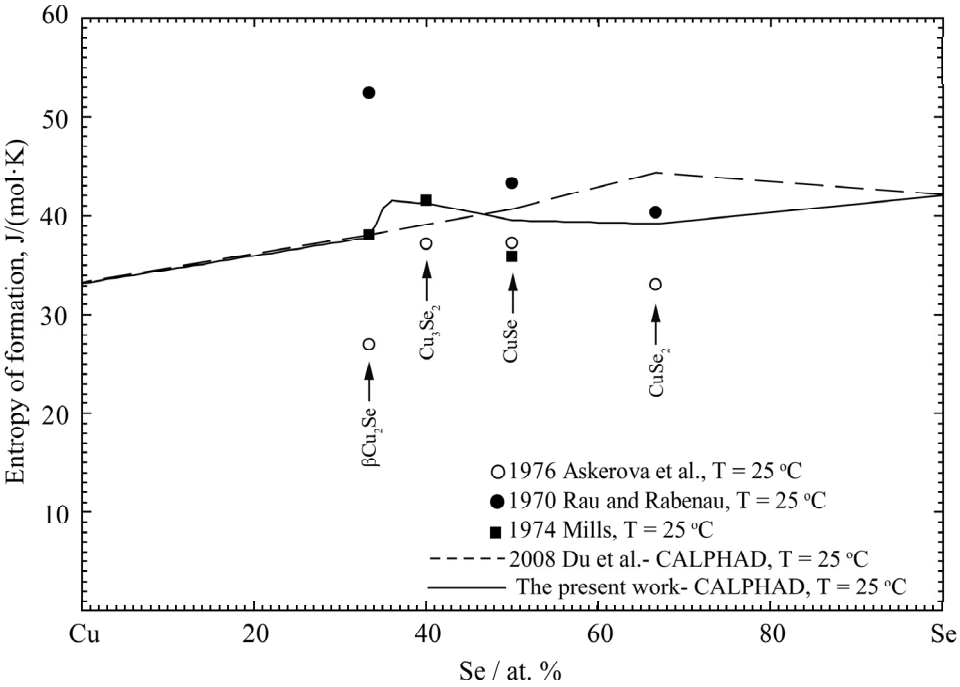

Figure 9. The calculated standard entropy of formation at 25 °C in the Cu-Se system compared with the experimental data from refs. [93–95] and previously optimized results by Du et al. [100].

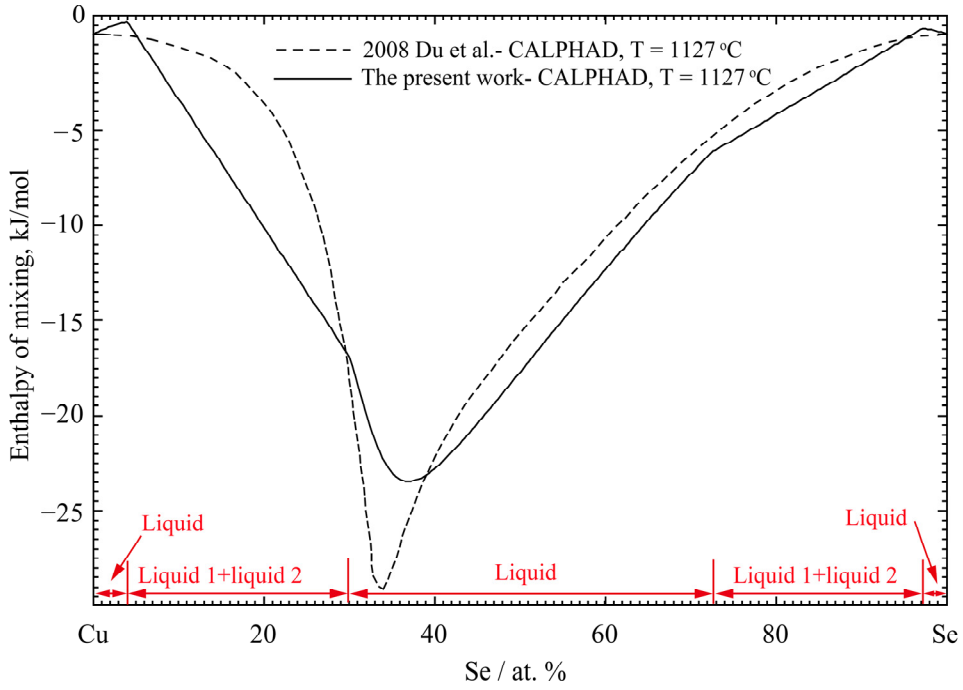

Figure 10. The calculated enthalpy of mixing for the liquid phase at 1127 °C in the Cu-Se system compared with previously optimized results by Du et al. [100].

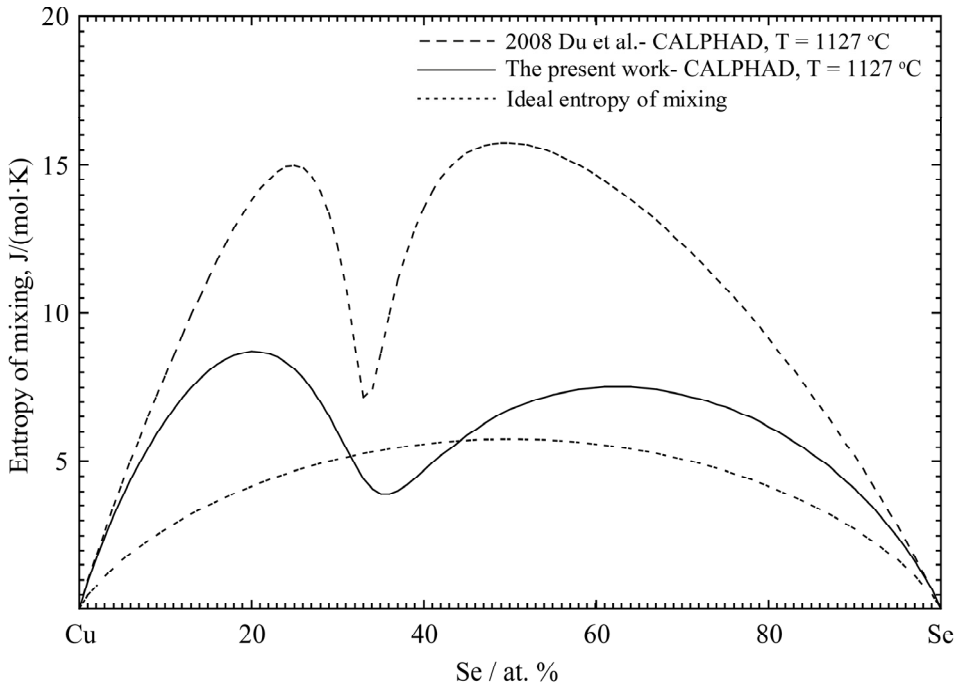

Figure 11. The calculated entropy of mixing for the liquid phase at 1127 °C in the Cu-Se system compared with the previously optimized results by Du et al. [100].

Figure 12 presents the calculated heat capacities of Cu_2Se in the Cu-Se system with the experimental data measured by Kubaschewski and Nolting [97] and Blachnik and Gunia [98], and the calculated results by Du et al. [100]. The present calculated results are in strong agreement with the experimental data in the present work. Figure 13 shows the calculated heat capacities of CuSe in the Cu-Se system compared with the experimental data measured by [96] and the calculated results by Du et al. [100]. The present calculated results show very strong agreement with the experimental data. The calculated activities

of Cu and Se at 1100 °C are shown in Figure 14, compared with the experimental data determined by Blachnik and Bolte [102] and the calculated by Du et al. [100].

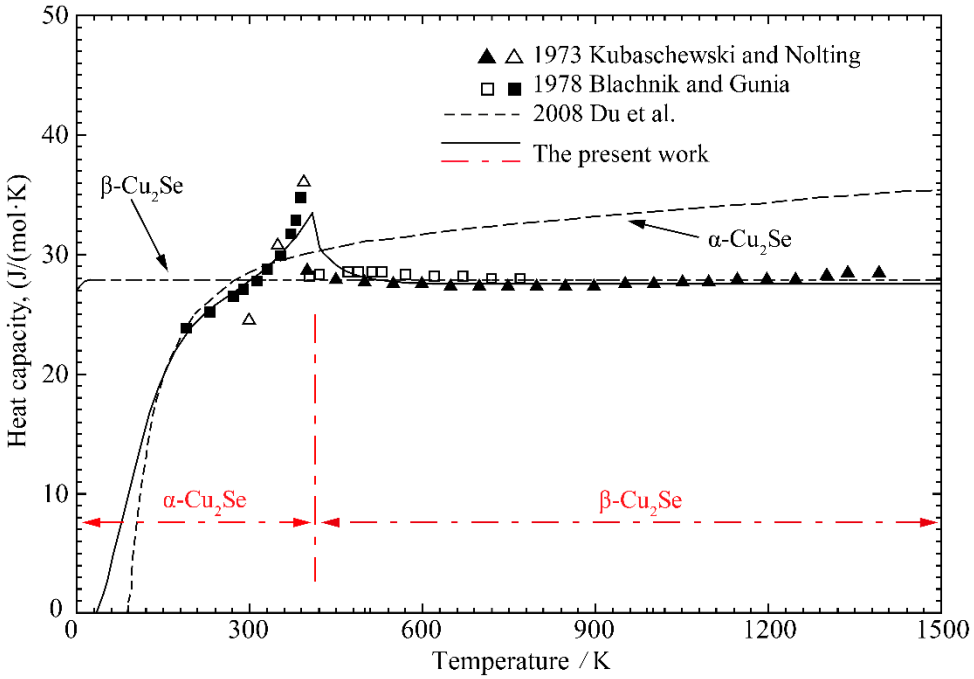

Figure 12. The calculated heat capacities of Cu_2Se in the Cu-Se system compared with the experimental data from refs. [97,98] and previously optimized results by Du et al. [100].

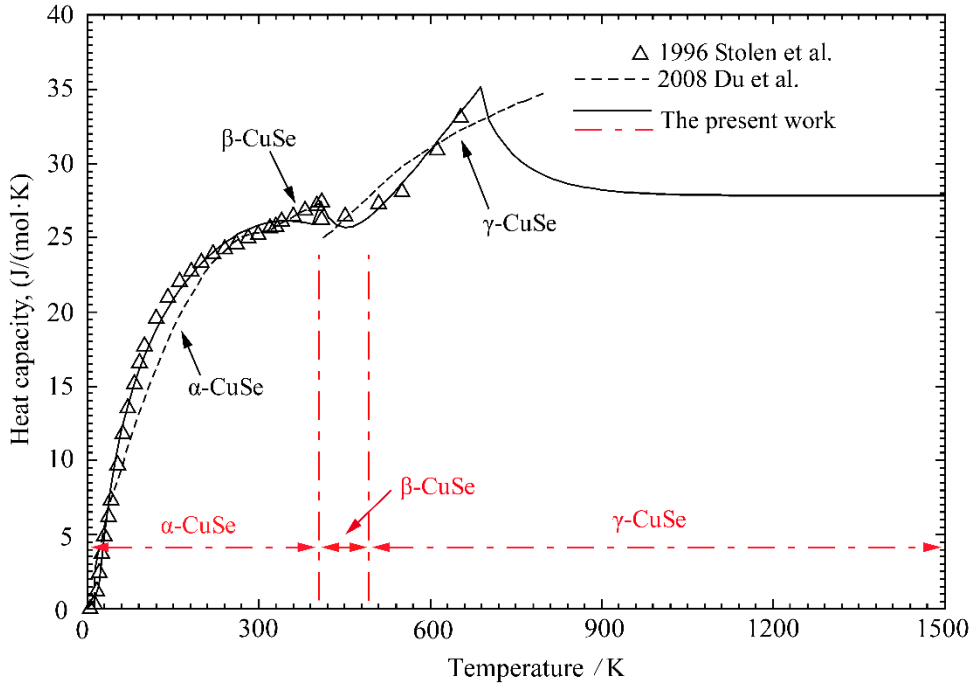

Figure 13. The calculated heat capacities of CuSe in the Cu-Se system compared with the experimental data from ref. [96] and previously optimized results by Du et al. [100].

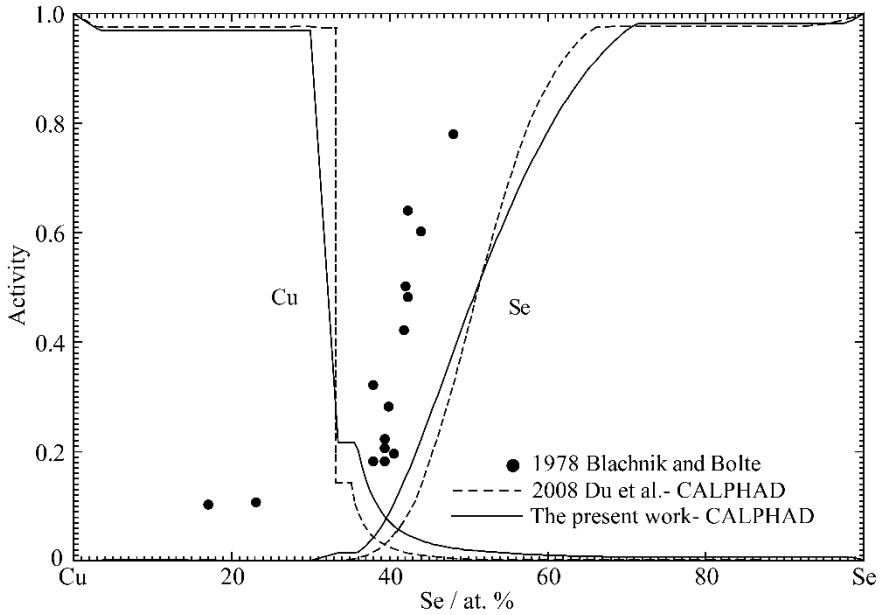

Figure 14. The calculated activities of Cu and Se at 1100 °C in the Cu-Se system compared with the experimental data from ref. [102] and previously optimized results by Du et al. [100].

4.3. Zn-Se Binary System

In the present work, the MQM model was used for liquid phase to optimize the Zn-Se binary system. The calculated phase diagram, compared with the experimental data [108,109,111,113] and optimized data [125], is shown in Figure 15, and it is in strong agreement with those data. Moreover, the melting point of ZnTe was optimized to be 1522 °C in the present work, thus reproducing the results reported by Okada et al. [104]. The calculated invariant reactions, together with the assessment results by Sharma and Chang [101] and optimized results by Chen et al. [125], are all listed in Table 9. It is worth noting that the calculated temperature and compositions of the monotectic reaction (Liquid#1 ↔ Liquid#2 + ZnSe) by Chen et al. [125] were inconsistent with the results of Sharma and Chang [101] and our results.

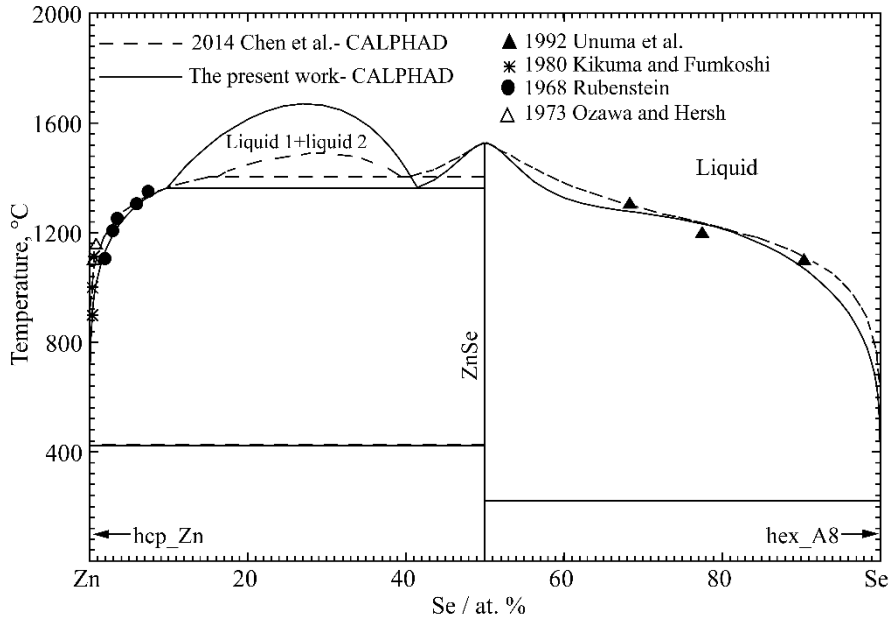

Figure 15. The calculated phase diagram of the Zn-Se system compared with the experimental data from refs. [108,109,111,113] and previously optimized results by Chen et al. [125].

Table 9. The calculated invariant reactions in Zn-Se system compared with experimental data from ref. [100] and calculated data from ref. [123].

Reaction	Reaction Type	Temperature (°C)	Composition (Zn at. %)			Refs.
Liquid#1 + fcc_A1 ↔ β-Cu2Se	Eutectic	419	0.0	0.0	50.0	[100]
		419	0.0	0.0	50.0	[123]
		419	0.0	0.0	50.0	This work
Liquid#1 ↔ liquid#2 + ZnSe	Monotectic	1360	10.9	42.6	50.0	[100]
		1402	16.0	40.0	50.0	[123]
		1363	9.8	41.5	50.0	This work
Liquid ↔ ZnSe + hex_A8	Eutectic	221	100.0	50.0	100.0	[100]
		221	100.0	50.0	100.0	[123]
		221	100.0	50.0	100.0	This work
Liquid ↔ ZnSe	Congruent	1526	50.0	50.0		[100]
		1526	50.0	50.0		[123]
		1525	50.0	50.0		This work

The calculated standard enthalpy and entropy of the formation of ZnSe at 25 °C in this work were compared with the averaged values of experimental results [103,116–124] and the optimized results by Chen et al. [125], and these are listed in Table 3. The present calculated result was slightly lower than that of Chen et al. [125], which was in closer agreement with experimental values. Figure 16 shows the calculated standard enthalpy of the formation of ZnSe at 25 °C, compared with the experimental results [106,118,123,133] and previously optimized results by Chen et al. [125]. The present calculated enthalpy showed better consistency with the experimental data [118,123,133]. The present calculated standard entropy of the formation of ZnSe at 25 °C, compared with the experimental results [118,123] and previously optimized results by Chen et al. [125], is shown in Figure 17. The present calculated result is slightly different from the experimental results, within the acceptable range.

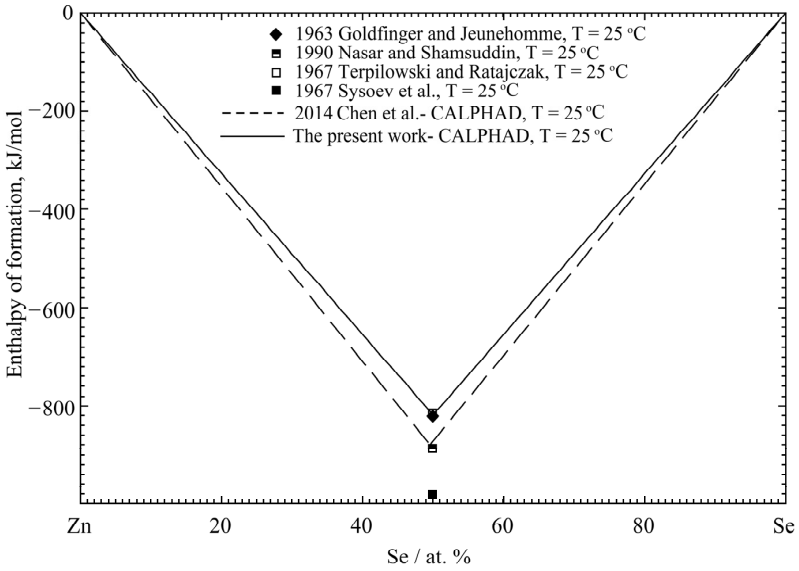

Figure 16. The calculated standard enthalpy of formation at 25 °C in the Zn-Se system compared with the experimental data from refs. [106,118,123,133] and previously optimized results by Chen et al. [125].

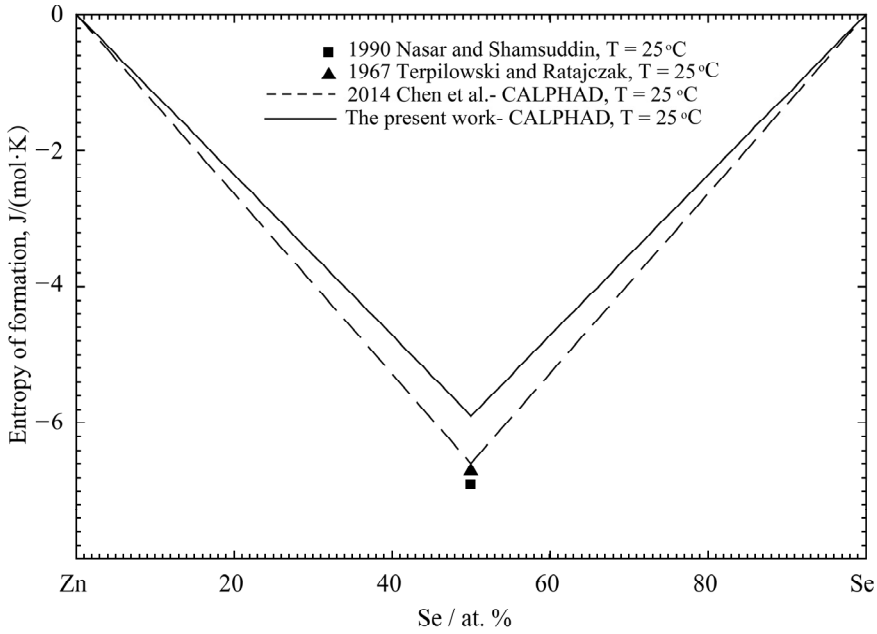

Figure 17. The calculated standard entropy of formation at 25 °C in the Zn-Se system compared with the experimental data from refs. [118,123] and previously optimized results by Chen et al. [125].

The calculated enthalpy and entropy of mixing for the liquid phase of the Zn-Se system at 1727 °C, compared with the calculated results by Chen et al. [125], are shown in Figures 18 and 19, respectively. The V-shaped enthalpy and M-shaped entropy curves indicate that the liquid phase had a maximum short-range order (SRO) at 50 at. % Se. Moreover, the calculated entropy results in this work are more consistent with the ideal state of the entropy of mixing than those calculated by Chen et al. [125].

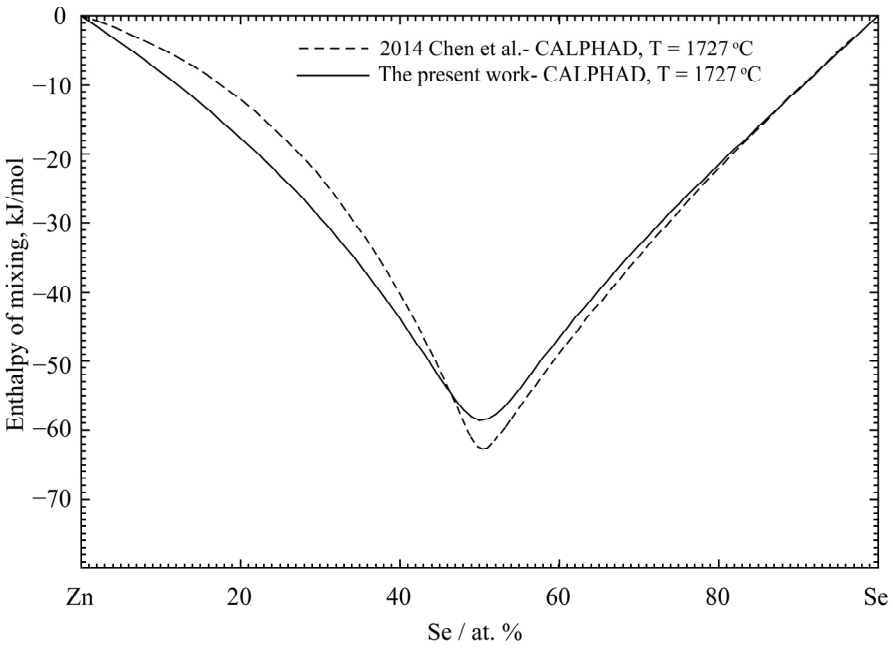

Figure 18. The calculated enthalpy of mixing at 1727 °C in the Zn-Se system compared with previously optimized results by Chen et al. [125].

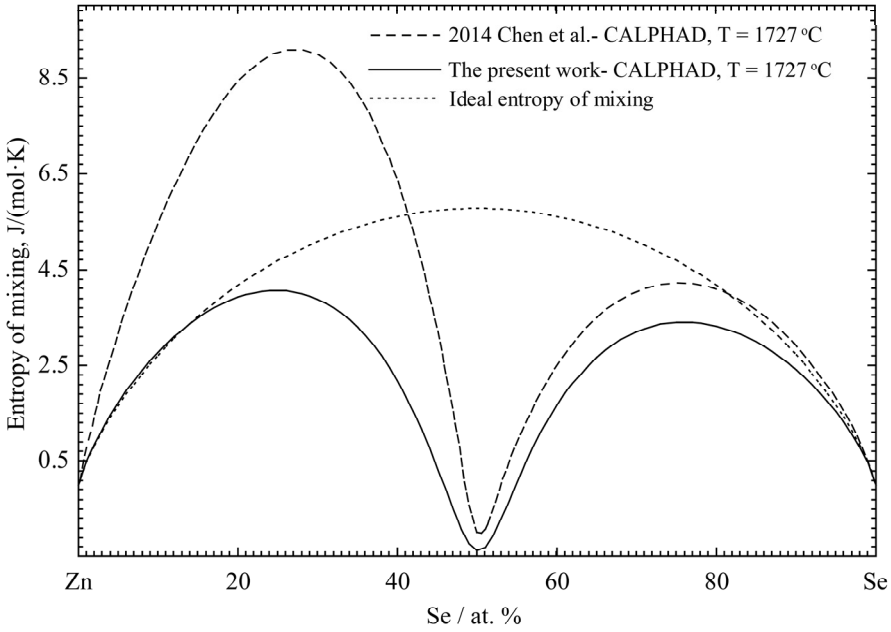

Figure 19. The calculated entropy of mixing at 1727 °C in the Zn-Se system compared with previously optimized results by Chen et al. [125].

5. Conclusions

Critical evaluations and thermodynamic reassessments of the Cu-Zn, Cu-Se and Zn-Se binary systems were conducted in the present work. The MQM method was applied to describe the Gibbs energy of the liquid phase. The Gibbs energies of all the intermetallic compounds and terminal solid solutions were described by the CEF method.

The critical literature assessment and thermodynamic re-optimization of the Cu-Zn binary system were carried out considering the ordered bcc_B2 crystal structure of the β' phase. The β and δ phases with the same bcc_A2 crystal structure were treated as one single phase. The $\gamma(Cu_5Zn_8)$ phase was modeled as four sub-lattices based on the information about the crystal structure and atomic distribution.

In the Cu-Se system, two miscibility gaps of the liquid were identified on each side of the compound Cu_2Se. The intermetallic compounds, Cu_3Se_2, α-CuSe, β-CuSe, γ-CuSe, $CuSe_2$ and α-Cu_2Se, were treated as stoichiometric compounds. The compound β-$Cu_{2-x}Se$, which has a homogeneity range, was treated using a two-sub-lattice model, $(Cu, Va)_2Se$.

In the Zn-Se system, two miscibility gaps of the liquid were identified in the Zn-rich and Se-rich regions. Only one intermediate phase, ZnSe, which is congruently formed, was treated as a stoichiometric compound in the present thermodynamic modeling. The Gibbs free energies of each phase were formulated in this work, which allowed the liquids, enthalpies of mixing, entropies of mixing, activities, enthalpies of formation and entropies of formation to be well represented.

A self-consistent thermodynamic database was constructed for the Cu-Zn, Cu-Se and Zn-Se binary systems, which formed part of the wider thermodynamic database research project conducted by our group on Mg/Zn-based multi-component systems [134–139]. Additionally, it provided reliable data supporting the search for ideal Zn-based biodegradable materials. Moreover, some of the experiments could be argued to verify the phase diagram (the miscibility gap) of the Se-rich part of the Cu-Se system and the Zn-Se system, although such experiments are difficult to perform due to the high volatility of Zn and Se.

Author Contributions: Conceptualization, J.M.; data curation, Y.T. and D.H.; investigation, Y.T. and D.H.; formal analysis, Y.T. and D.H.; writing—original draft, Y.T.; software, Y.T.; validation, J.W. and L.J.; writing—review and editing, J.M., J.W. and H.Q.; supervision, H.Q. and L.J.; funding acquisition, J.M. and H.Q. All authors have read and agreed to the published version of the manuscript.

Funding: This research was funded by the Natural Science Foundation of Anhui Province, 2108085QE213, the Nature Science Foundation of the Universities of Anhui Province, KJ2019A0776, and the special innovation projects of universities in the Guangdong Province, 2018KTSCX240.

Institutional Review Board Statement: Not applicable.

Informed Consent Statement: Not applicable.

Data Availability Statement: Not applicable.

Conflicts of Interest: The authors declare no conflict of interest.

References

1. Frederickson, C.J.; Koh, J.-Y.; Bush, A.I. The neurobiology of zinc in health and disease. *Nat. Rev. Neurosci.* **2005**, *6*, 449–462. [CrossRef] [PubMed]
2. Seitz, J.M.; Durisin, M.; Goldman, J.; Drelich, J.W. Drelich Recent Advances in Biodegradable Metals for Medical Sutures: A Critical Review. *Adv. Healthc. Mater.* **2015**, *4*, 1915–1936. [CrossRef] [PubMed]
3. Hernández, E.; Champagne, D.; Yilmazer, S.; Dikici, H.; Boehlert, B.; Hermawan, C.J.; Biomaterialia, H.J.A. Current status and perspectives of zinc-based absorbable alloys for biomedical applications. *Acta Biomater.* **2019**, *97*, 1–22. [CrossRef] [PubMed]
4. Mostaed, E.; Sikora-Jasinska, E.; Drelich, M.; Vedani, J.W.; Maurizio, V. Zinc-based alloys for degradable vascular stent applications. *Acta Biomater.* **2018**, *71*, 1–23. [CrossRef] [PubMed]
5. Venezuela, J.J.D.; Johnston, S.; Dargusch, M.S. The prospects for biodegradable zinc in wound closure applications. *Acta Biomater.* **2019**, *8*, 1900408. [CrossRef]
6. Dambatta, M.; Kurniawan, D.; Izman, S.; Yahaya, B.; Hermawan, H. Review on Zn-Based Alloys As Potential Biodegradable Medical Devices Materials. In *Applied Mechanics and Material*; Trans Tech Publications Ltd.: New York, NY, USA, 2015; Volume 776, pp. 277–281.
7. Katarivas Levy, G.; Goldman, J.; Aghion, E.J.M. The prospects of zinc as a structural material for biodegradable implants—A review paper. *Biodegr. Metals* **2017**, *7*, 402. [CrossRef]
8. Čapek, J.; Jablonská, E.; Lipov, J.; Kubatík, T.F.; Vojtěch, D. Physics. Preparation and characterization of porous zinc prepared by spark plasma sintering as a material for biodegradable scaffolds. *Mater. Chem. Phys.* **2018**, *203*, 249–258. [CrossRef]
9. Zhao, L.; Wang, X.; Wang, T.; Xia, Y.; Cui, C. Mechanical properties and biodegradation of porous Zn-1Al alloy scaffolds. *Mater. Lett.* **2019**, *247*, 75–78. [CrossRef]
10. Tang, Z.; Niu, J.; Huang, H.; Zhang, H.; Pei, J.; Ou, J.; Yuan, G. Potential biodegradable Zn-Cu binary alloys developed for cardiovascular implant applications. *J. Mech. Behav. Biomed. Mater.* **2017**, *72*, 182–191. [CrossRef]
11. Xiao, X.; Liu, E.; Shao, J.; Ge, S. Advances on biodegradable zinc-silver-based alloys for biomedical applications. *J. Appl. Biomater.* **2021**, *19*, 22808000211062407. [CrossRef]
12. Su, Y.; Cockerill, I.; Wang, Y.; Qin, Y.-X.; Chang, L.; Zheng, Y.; Zhu, D. Zinc-based biomaterials for regeneration and therapy. *Trends Biotechnol.* **2019**, *37*, 428–441. [CrossRef] [PubMed]
13. Venezuela, J.; Dargusch, M. The influence of alloying and fabrication techniques on the mechanical properties, biodegradability and biocompatibility of zinc: A comprehensive review. *Acta Biomater.* **2019**, *87*, 1–40. [CrossRef] [PubMed]
14. Yuan, W.; Xia, D.; Wu, S.; Zheng, Y.; Guan, Z.; Rau, J.V. A review on current research status of the surface modification of Zn-based biodegradable metals. *Bioact. Mater.* **2022**, *7*, 192–216. [CrossRef] [PubMed]
15. Li, P.; Schille, C.; Schweizer, E.; Kimmerle-Müller, E.; Rupp, F.; Heiss, A.; Legner, C.; Klotz, U.E.; Geis-Gerstorfer, J.; Scheideler, L. Selection of extraction medium influences cytotoxicity of zinc and its alloys. *Acta Biomater.* **2019**, *98*, 235–245. [CrossRef]
16. Li, H.; Yang, H.; Zheng, Y.; Zhou, F.; Qiu, K.; Wang, X. Design and characterizations of novel biodegradable ternary Zn-based alloys with IIA nutrient alloying elements Mg, Ca and Sr. *Mater. Des.* **2015**, *83*, 95–102. [CrossRef]
17. Zhang, Y.; Li, Q.; Guo, T.; Li, S. Effect of Y Content on Properties of Extruded Zn-1.5Mg-xY Alloys for Medical Applications. *Mater. Res.* **2019**, *22*, 95–103. [CrossRef]
18. Shi, Z.-Z.; Yu, J.; Liu, X.-F.; Zhang, H.-J.; Zhang, D.-W.; Yin, Y.-X.; Wang, L.-N. Effects of Ag, Cu or Ca addition on microstructure and comprehensive properties of biodegradable Zn-0.8Mn alloy. *Mater. Sci. Eng. C* **2019**, *99*, 969–978. [CrossRef]
19. Chen, H.T.; Shi, Z.Z.; Liu, X.F. Microstructure and mechanical properties of extruded and caliber rolled biodegradable Zn-0.8Mn-0.4Ag alloy with high ductility. *Mater. Sci. Eng. A* **2020**, *770*, 138543. [CrossRef]
20. Bednarczyk, W.; Kawałko, J.; Wątroba, M.; Bała, P. Achieving room temperature superplasticity in the Zn-0.5Cu alloy processed via equal channel angular pressing. *Mater. Sci. Eng. A* **2018**, *723*, 126–133. [CrossRef]
21. Niu, J.; Tang, Z.; Huang, H.; Jia Pei, H.Z.; Yuan, G.; Ding, W. Research on a Zn-Cu alloy as a biodegradable material for potential vascular stents application. *Mater. Sci. Eng. C* **2016**, *69*, 407–413. [CrossRef]
22. Fairweather-Tait, S.J.; Bao, Y.; Broadley, M.R.; Collings, R.; Ford, D.; Hesketh, J.E.; Hurst, R. Selenium in Human Health and Disease. *Antioxid. Redox Signal.* **2011**, *14*, 1337–1383. [CrossRef] [PubMed]
23. Kipp, A.P.; Strohm, D.; Brigelius-Flohé, R.; Schomburg, L.; Bechthold, A.; Leschik-Bonnet, E.; Heseker, H. Revised reference values for selenium intake. *J. Trace Elem. Med. Biol.* **2015**, *32*, 195–199. [CrossRef] [PubMed]

24. Gemma, F.-M.; Ana, N.-A.; Roberto, P.-B.; Eliseo, G. Selenium and coronary heart disease: A meta-analysis. *Am. J. Clin. Nutr.* **2006**, *84*, 762–763.
25. Rederstorff, M.; Krol, A.; Lescure, A. Understanding the importance of selenium and selenoproteins in muscle function. *Cell. Mol. Life Sci.* **2006**, *63*, 52–59. [CrossRef] [PubMed]
26. Shanu, A.; Groebler, L.; Kim, H.B.; Wood, S.; Weekley, C.M.; Aitken, J.B.; Harris, H.H.; Witting, P.K. Selenium Inhibits Renal Oxidation and Inflammation But Not Acute Kidney Injury in an Animal Model of Rhabdomyolysis. *Antioxid. Redox Signal.* **2013**, *18*, 756–769. [CrossRef]
27. Wang, Y.; Wu, Y.; Luo, K.; Liu, Y.; Zhou, M.; Yan, S.; Shi, H.; Cai, Y. The protective effects of selenium on cadmium-induced oxidative stress and apoptosis via mitochondria pathway in mice kidney. *Food Chem. Toxicol.* **2013**, *58*, 61–67. [CrossRef]
28. Joshi, D.; Mittal, D.K.; Shukla, S.; Srivastav, A.K.; Srivastav, S.K. N-acetyl cysteine and selenium protects mercuric chloride-induced oxidative stress and antioxidant defense system in liver and kidney of rats: A histopathological approach. *J. Trace Elem. Med. Biol.* **2014**, *28*, 218–226. [CrossRef]
29. Persaud-Sharma, D.; Budiansky, N.; McGoron, A.J. Biocompatibility Assessment of Novel Bioresorbable Alloys Mg-Zn-Se and Mg-Zn-Cu for Endovascular Applications: In-Vitro Studies. *J. Biomater. Tiss. Eng.* **2013**, *17*, 25–43. [CrossRef]
30. Saunders, N.; Miodownik, A.P. *Calphad (Calculation of Phase Diagrams) A Comprehensive Guide*; Pergamon: Oxford, UK, 1992.
31. Jin, L.; Kang, Y.B.; Chartrand, P.; Fuerst, C.D.J.C. Thermodynamic evaluation and optimization of Al-La, Al-Ce, Al-Pr, Al-Nd and Al-Sm systems using the modified quasichemical model for liquids. *Calphad* **2011**, *35*, 30–41. [CrossRef]
32. Hillert, M. The compound energy formalism. *J. Alloys Compd.* **2001**, *320*, 161–176. [CrossRef]
33. Shepherd, E.S. The Constitution of Copper Zinc Alloys. *J. Phys. Chem. C* **1904**, *8*, 421–435. [CrossRef]
34. Hoyt, S.L. On the Copper-rich Kalchoids (copper-tin-zinc-alloys). *J. Inst. Met.* **1913**, *10*, 235.
35. Campbell, W. A note on the constitution of certain tin-bearing brasses. Master Thesis, Columbia University, New York, NY, USA, 1920.
36. Bauer, O.; Hansen, M. *Der Aufbau der Kupfer-Zinklegierungen*; Springer: Berlin/Heidelberg, Germany, 1927.
37. Ruer, R.; Kremers, K. Das System Kupfer-Link. *Z. Anorg. Allg. Chem.* **1929**, *184*, 193–231. [CrossRef]
38. Schramm, J. Contribution to the Cu-Zn diagram. *Prog. Mater. Sci.* **1935**, *14*, 995–1001.
39. Hansen, M. *Handbook of Binary Alloys*; Springer: Berlin, Germany, 1936.
40. Raynor, G. The Cu-Sn Phase Diagram. *Annot. Equilib. Diagr. Ser.* **1944**, *2*, 4–5.
41. Hansen, M.; Anderko, K. *Constitution of Binary Alloys*; McGraw-Hill: New York, USA, 1958.
42. Massalski, T.; Okamoto, H.; Subramanian, D.; Kacprzak, L.; Scott, W. *Binary Alloy Phase Diagrams*; American Society for Metals: Park, OH, USA, 1986.
43. Miodownik, A. Phase diagrams of binary copper alloys. *ASM Int.* **1994**, *10*, 487–496.
44. Spencer, P. A thermodynamic evaluation of the Cu-Zn system. *Calphad* **1986**, *10*, 175–185. [CrossRef]
45. Kowalski, M.; Spencer, P. Thermodynamic reevaluation of the Cu-Zn system. *J. Phase Equilib.* **1993**, *14*, 432–438. [CrossRef]
46. Liang, H.; Chang, Y.A. A Thermodynamic Description for the Al-Cu-Zn System. *J. Phase Equilib.* **1998**, *19*, 25–37. [CrossRef]
47. David, N.; Fiorani, J.; Vilasi, M.; Hertz, J. Thermodynamic reevaluation of the Cu-Zn system by electromotive force measurements in the zinc-rich part. *J. Phase Equilib.* **2003**, *24*, 240–248. [CrossRef]
48. Gierlotka, W.; Chen, S. Thermodynamic descriptions of the Cu–Zn system. *J. Mater. Res.* **2008**, *23*, 258–263. [CrossRef]
49. Wang, J.; Xu, H.; Shang, S.; Zhang, L.; Yong, D.; Zhang, W.; Liu, S.; Wang, P.; Liu, Z. Experimental investigation and thermodynamic modeling of the Cu-Si-Zn system with the refined description for the Cu-Zn system. *Calphad* **2011**, *35*, 191–203. [CrossRef]
50. Liang, S.; Hsiao, H.; Fetzer, R. Thermodynamic assessment of the Al–Cu–Zn system, part I: Cu–Zn binary system. *Calphad* **2015**, *51*, 224–232. [CrossRef]
51. Saunders, N. COST 507: Thermochemical database for light metal alloys. *COST* **1998**, *168*, 23–27.
52. Bradley, A.; Gregory, C.I.X. A comparison of the crystal structures of Cu_5Zn_8 and Cu_5Cd_8. *Lond. Edinb. Dublin Philos. Mag. J. Sci.* **1931**, *12*, 143–162. [CrossRef]
53. Heidenstam, O.; Johansson, A.; Westman, S.; Larsen, C. A Redetermination of the Distribution of Atoms in Cu_5Zn_8, Cu_5Cd_8, and Cu_9Al_4. *Acta Chem. Scand.* **1968**, *22*, 653–661. [CrossRef]
54. Gourdon, O.; Gout, D.; Williams, D.; Proffen, T.; Hobbs, S.; Miller, G. Atomic distributions in the gamma-brass structure of the Cu-Zn system: A structural and theoretical study. *Inorg. Chem.* **2007**, *46*, 251–260. [CrossRef] [PubMed]
55. Sehubert, K.; Wall, E. Zur Kristallstruktur der δ-Hochtemperaturphase des Systems Kupfer-Zink. *Int. J. Mater. Res.* **1949**, *40*, 383–385. [CrossRef]
56. Lenz, J.; Schubert, K. Über einige Leerstellen-und Stapelvarianten der Beta-Messing Strukturfamilie. *Int. J. Mater. Res.* **1971**, *62*, 810–816. [CrossRef]
57. Degtyareva, V.F.; Afonikova, N.S. Simple metal binary phases based on the body centered cubic structure: Electronic origin of distortions and superlattices. *J. Phys. Chem. Solids* **2013**, *74*, 18–24. [CrossRef]
58. Parameswaran, K.; Healy, G. A Calorimetric Investigation of the Copper-Zinc System. *Metall. Trans. B* **1978**, *9*, 657–664. [CrossRef]
59. Turchanin, M. Enthalpies of formation of liquid copper alloys with 3d transition metals. *Russ. Metall.* **1998**, *4*, 29–38.
60. Samson-Himmelstjerna, H.O. Heat capacity and heat of formation of molten alloys. *Z. Metallkd.* **1936**, *28*, 197.
61. Schneider, A.; Schmid, H. Die Dampfdrucke des Zinks und Cadmiums über ihren binären flüssigen Legierungen mit Kupfer, Silber und Gold. Metalldampfdrucke III. *Z. Für Elektrochem. Ber. Der Bunsenges. Für Phys. Chem.* **1942**, *48*, 627–639.

62. Everett, L.H.; Jacobs, P.W.M.; Kitchener, J.A. The activity of zinc in liquid copper-zinc alloys. *Acta Metall.* **1957**, *5*, 281–284. [CrossRef]
63. Downie, D. Thermodynamic and structural properties of liquid zinc/copper alloys. *Acta Metall.* **1964**, *12*, 875–882. [CrossRef]
64. Azakami, T.; Yazawa, A. Thermodynamic Studies of Liquid Copper Alloys. III. Activities of Zinc and Cadmium in Liquid Copper-Base Alloys. *J. I. Min. Metal.* **1968**, *84*, 1663–1668.
65. Solovev, S.; Knyazev, M.; Ivanov, Y.; Vanyukov, A. Mass spectrometric study of partial characteristics of zinc in copper-zinc system. *Ind. Lab. (USSR)* **1979**, *45*, 841–844.
66. Sugino, S.; Hagiwara, H. Activity of Zinc in Molten Copper and Copper-Gold Alloys. *J. Jpn. Inst. Met.* **1986**, *50*, 186–192. [CrossRef]
67. Leitgebel, W. Uber das Sieden einiger Metalle und Legierungen bei Atmospharendruck. *Z. Anorg. Allg. Chem.* **1931**, *202*, 305–324. [CrossRef]
68. Baker, E.H. Vapor pressures and thermodynamic behavior of liquid zinc–copper alloys at 1150 °C. *Trans. Inst. Min. Metall.* **1970**, *79*, C1–C2.
69. Kleppa, O.J.; Thalmayer, C.E. An EMF Investigation of Binary Liquid Alloys Rich in Zinc. *J. Phys. Chem.* **1959**, *63*, 1953–1958. [CrossRef]
70. Gerling, U.; Predel, B. Thermodynamic properties of liquid copper-zinc alloys. *Chem. Inf.* **1980**, *71*, 158–164.
71. Korber, F.; Oelsen, W. The formation enthalpy of the binary alloys Fe-Sb, Co-Sb, Ni-Sb, Co-Sn, Ni-Sn, Cu-Sn and Cu-Zn in the cast condition. *Mitt. Kaiser Wilhelm Inst. Eisenforsch.* **1937**, *19*, 158–164.
72. Weibke, F. Beiträge zur systematischen Verwandtschaftslehre. 71. Über die Bildungswärmen im System Kupfer-Zink. *Z. Anorg. Allg. Chem.* **1937**, *232*, 289–296. [CrossRef]
73. Kleppa, O.; King, R. Heat of formation of the solid solutions of zinc, gallium and germanium in copper. *Acta Metall.* **1962**, *10*, 1183–1186. [CrossRef]
74. Orr, R.; Argent, B. Heats of formation of the α-brasses. *Trans. Faraday Soc.* **1965**, *61*, 2126–2131. [CrossRef]
75. Blair, G.R.; Downie, D.B. A Calorimetric Study of Silver-Zinc and Copper-Zinc Alloys. *Met. Metall. Trus.* **1970**, *4*, 1–5. [CrossRef]
76. Ölander, A. Eine elektrochemische Untersuchung von Messing. *Z. Phys. Chem.* **1933**, *163*, 428–438. [CrossRef]
77. Seith, W.; Krauss, W. The diffusion and vapour pressure in zinc in brasses. *Z. Elektrochem.* **1938**, *44*, 98–102.
78. Hargreaves, R. The vapour pressure of zinc in brasses. *J. Inst. Met.* **1939**, *64*, 115–125.
79. Argent, B.B.; Wakeman, D.W. Thermodynamic properties of solid solutions. Part 1. Copper-zinc solid solution. *Trans. Faraday Soc.* **1958**, *54*, 799–806. [CrossRef]
80. Pemsler, J.P.; Rapperpo, E.J. Thermodynamic activity measurements using atomic absorption-copper-zinc. *Trans. Metall. S. A* **1969**, *245*, 1395.
81. Masson, D.; Sheu, J. Variations in the composition dependence of the activity coefficient in terminal solid solutions of Ag-Zn, Ag-Cd, and Cu-Zn. *Metall. Trans.* **1970**, *1*, 3005–3009. [CrossRef]
82. Heyding, R.D. The copper/selenium system. *Can. J. Chem.* **1966**, *44*, 1233–1236. [CrossRef]
83. Bernardini, G.P.; Corsini, F.; Trosti, R. Nuove relazioni di fase nel sistema Cu-Se. *Period. Mineral.* **1972**, *41*, 565–586.
84. Murray, R.M.; Heyding, R.D. The copper–selenium system at temperatures to 850 K and pressures to 50 kbar. *Can. J. Chem.* **1975**, *53*, 878–887. [CrossRef]
85. Babitsyna, A.A.; Emel'yanova, T.; Chernitsyna, M.A. Copper-Selenium System. *Zh. Neorg. Khim.* **1975**, *20*, 3093–3096.
86. Glazov, V.M.; Kim, S.G. Acoustic Studies of Liquid Immiscibility in the Cu-Se System. *Izv. Akad. Nauk. SSSR Neorg. Mater.* **1990**, *26*, 2488–2490.
87. Glazov, V.M.; Pavlova, L.M.; Asryan, A.A. Thermal Dissociation of Copper Chalcogenides during Melting. *Zh. Fiz. Khim.* **1996**, *70*, 232–236.
88. Glazov, V.M.; Pashinkin, A.S. Phase equilibria in the Cu-Se system. *Inorg. Mater.* **2000**, *36*, 641–652. [CrossRef]
89. Ogorelec, Z.; Mestnik, B.; Devčič, D. A new contribution to the equilibrium diagram of the Cu-Se system. *J. Mater. Sci.* **1972**, *7*, 967–969. [CrossRef]
90. Chakrabarti, D.; Laughlin, D. The Cu-Se (Copper-Selenium) system. *Bull. Alloy. Phase Diagr.* **1981**, *2*, 305–315. [CrossRef]
91. Muhsin, I. Thermodynamic stability and homogeneity of cuprous selenide by emf and coulometric titration. *Solid State Ion.* **2019**, *329*, 140–148.
92. Gattow, G.; Schneider, A. Die Bildungsenthalpien im System Kupfer-Selen. *Z. Anorg. Allg. Chem.* **1956**, *286*, 296–306. [CrossRef]
93. Askerova, K.A.; Alieva, N.A.; Azizov, T.K.; Abbasov, A.S.; Mustafayev, F.M. Thermodynamic Properties of Copper Selenides. *Izv. Akad. Nauk. Azerb. SSR* **1976**, *6*, 137–139.
94. Rau, H.; Rabenau, A. Vapour Pressure Measurements in the Copper-Selenium System. *J. Solid State Chem.* **1970**, *1*, 515–518. [CrossRef]
95. Mills, K.C. *Butterworths*; Butterworths Law: London, UK; Boston, MA, USA, 1974.
96. Stølen, S.; Fjellvag, H.; Grønvold, F.; Sipowska, J.T.; Westrum, J.E.F. Heat capacity, structural and thermodynamic properties of synthetic klockmannite CuSe at temperatures from 5 K to 652.7 K. Enthalpy of decomposition. *J. Chem. Thermodyn.* **1996**, *28*, 753–766. [CrossRef]
97. Kubaschewski, P.; Nölting, J. Spezifische Wärmen und thermische Fehlordnung von Kupferchalkogeniden Teil I: Cu2Se und Cu2Te bei angenähert stöchiometrischer Zusammensetzung. *Ber. Der Bunsenges. Für Phys. Chem.* **1973**, *77*, 70–74.

98. Blachnik, R.; Gunia, P.G. Enthalpien von Kupfer- und Silberchalkogeniden / Enthalpies of Copper and Silver Chalcogenides. *Z. Für Nat. A* **1978**, *33*, 190–196. [CrossRef]
99. Glazov, V.; Mendelevich, A.Y. Entropy of Melting of Silver and Copper Chalcogenides. *Elektron. Tekh. Ser.* **1968**, *1*, 114–119.
100. Du, Z.; Guo, C.; Tao, M.; Li, C. Thermodynamic modeling of the Cu-Se system. *Int. J. Mater. Res.* **2008**, *99*, 294–300. [CrossRef]
101. Sharma, R.C.; Chang, Y.A. The Se-Zn (Selenium-Zinc) System. *J. Phase Equilib.* **1996**, *17*, 155–160. [CrossRef]
102. Blachnik, R.; Bolte, G. Aktivitäten von Se in geschmolzenen Cu-Se und Ag-Se Mischungen. *J. Less Common Met.* **1978**, *57*, 21–28. [CrossRef]
103. Brebrick, R.; Liu, H. Analysis of the Zn-Se System. *J. Phase Equilib.* **1996**, *17*, 495–501. [CrossRef]
104. Okada, H.; Kawanaka, T.; Ohmoto, S. Study on the ZnSe phase diagram by differential thermal analysis. *J. Cryst. Growth* **1996**, *165*, 31–36. [CrossRef]
105. Fischer, A.G. Preparation and Properties of ZnS-Type Crystals from the Melt. *J. Electrochem. Soc.* **1959**, *106*, 838. [CrossRef]
106. Sysoev, L.; Raiskin, E.; Gur'ev, V. Measurement of the Melting Point of Sulfides, Selenides, and Tellurides of Zn and Cd. *Izv. Akad. Nauk SSSR Neorg. Mater.* **1967**, *3*, 390–391.
107. Sharma, R.; Chang, Y. Thermodynamic analysis and phase equilibria calculations for the Zn-Te, Zn-Se and Zn-S systems. *J. Cryst. Growth* **1988**, *88*, 193–204. [CrossRef]
108. Rubenstein, M. Solution growth of some II-VI compounds using tin as a solvent. *J. Cryst. Growth* **1968**, *3*, 309–312. [CrossRef]
109. Ozawa, L.; Hersh, H.N. Resistivity and Photoluminescence of Zn(S, Se):l Annealed in Liquid Zinc. *J. Electrochem. Soc.* **1973**, *120*, 935–942. [CrossRef]
110. Kuzhelev, L.; Mironov, I.; Pavlova, V.; Stroganova, I. Solubility of the selenium and tellurium in zinc in the range 700–1100 °C. *J. Phys. Chem* **1974**, *48*, 287.
111. Kikuma, I.; Furukoshi, M. Solution growth of ZnSe crystals using In-Zn solvents. *J. Cryst. Growth* **1980**, *50*, 654–658. [CrossRef]
112. Nakamura, H.; Sun, L.Y.; Asano, A.; Nakamura, Y.; Washiyama, M.; Aoki, M. Liquid-phase epitaxial growth of ZnSe on ZnTe substrate. *Jpn. J. Appl. Phys.* **1983**, *22*, 499–503. [CrossRef]
113. Unuma, H.; Higuchi, M.; Yamakawa, Y.; Kodaira, K.; Koyama, T. Liquid Encapsulated Flux Growth of ZnSe Single Crystals from Se Solvent. *Jpn. J. Appl. Phys.* **1992**, *31*, L383. [CrossRef]
114. Sharma, R.; Chang, Y. The Te−Zn (Tellurium-Zinc) system. *Bull. Alloy. Phase Diagr.* **1987**, *8*, 14–19. [CrossRef]
115. Korneeva, I.; Sokolov, V.; Novoselova, A. Saturated-vapor pressure of zinc and cadmium selenides in the solid state. *Russ. J. Inorg. Chem.* **1960**, *5*, 117–119.
116. Wosten, W.J.; Geers, M.G. The vapor pressure of zinc selenide. *J. Phys. Chem.* **1961**, *66*, 1252–1253. [CrossRef]
117. Sedgwick, T.O.; Agule, B.J. Bourdon Gauge Determination of Equilibrium in the ZnSe(s)-12(g) System. *J. Electrochem. Soc.* **1966**, *113*, 54–57. [CrossRef]
118. Terpilowski, J.; Ratajczak, E. Thermodynamic Properties of Zinc Selenide. *Roczn. Chem.* **1967**, *41*, 429–433.
119. Flögel, P. Zur Kristallzüchtung von Cadmiumsulfid und anderen II-IV-Verbindungen. III. Zum Gleichgewicht zwischen Selen und Wasserstoff bei 1000 °C. *Z. Anorg. Allg. Chem.* **1969**, *370*, 16–30. [CrossRef]
120. Hassan, M.; Munir, Z.A. Studies on the Sublimation of IIB-VIA Compounds. VI. Thermodynamics of the Dissociation of Zinc Selenide. *High Temper.* **1973**, *5*, 34–39.
121. Kirk, D.; Raven, M. A theory dealing with the vacuum evaporation and deposition of binary semiconducting compounds, with special reference to the thermal evaporation of zinc selenide. *J. Phys. D Appl. Phys.* **1976**, *9*, 2015. [CrossRef]
122. Bardi, G.; Trionfetti, G. Vapour pressure and sublimation enthalpy of zinc selenide and zinc telluride by thermogravimetric knudsen-effusion method. *Thermochim. Acta* **1990**, *157*, 287–294. [CrossRef]
123. Nasar, A.; Shamsuddin, M. Thermodynamic Properties of Zinc Selenide Thermodynamische Eigenschaften von Zinkselenid. *Int. J. Mater. Res.* **1990**, *81*, 244–246. [CrossRef]
124. Schönherr, E.; Freiberg, M.; Siche, D.; Hartmann, H. The vapor composition and vapor pressure of ZnSe from a modified Knudsen technique between 1190 and 1310 K. *Ber. Der Bunsenges. Für Phys. Chem.* **1996**, *100*, 1766–1771. [CrossRef]
125. Yang, C.; Liu, Y.; Chu, M.; Wang, L. Phase diagrams and thermodynamic descriptions for the Bi–Se and Zn–Se binary systems. *J. Alloys Compd.* **2014**, *617*, 423–428.
126. Bale, C.W.; Chartrand, P.; Degterov, S.A.; Eriksson, G.; Hack, K.; Mahfoud, R.B.; Melancon, J.; Pelton, A.D.; Petersen, S. FactSage Thermochemical Software and Databases. *Calphad Pergamon Press* **2002**, *26*, 189–228. [CrossRef]
127. Dinsdale, A.T. SGTE data for pure elements. *Calphad* **1991**, *15*, 317–425. [CrossRef]
128. Pelton, A.D.; Degterov, S.A.; Eriksson, G.; Robelin, C.; Dessureault, Y. The modified quasichemical model I—Binary solutions. *Metall. Mater. Trans. B* **2000**, *31*, 651–659. [CrossRef]
129. Pelton, A.D.; Chartrand, P. The modified quasi-chemical model: Part II. Multi-component solutions. *Metall. Mater. Trans. A* **2001**, *32*, 1355–1360. [CrossRef]
130. Kang, Y.B.; Pelton, A.D.; Chartrand, P.; Fuerst, C.D. Critical evaluation and thermodynamic optimization of the Al-Ce, Al-Y, Al-Sc and Mg-Sc binary systems. *Calphad* **2008**, *32*, 413–422. [CrossRef]
131. Dupin, N.; Ansara, I. On the sublattice formalism applied to the B2 phase. *Z. Metallk.* **1999**, *90*, 76–85.
132. Kopp, H.J. Investigations of the specific heat of solid bodies. *J. Chem. Soc.* **1866**, *19*, 154–234. [CrossRef]
133. Goldfinger, P.; Jeunehomme, M. Mass spectrometric and Knudsen-cell vaporization studies of group 2B-6B compounds. *Trans. Faraday Soc.* **1963**, *59*, 2851–2867. [CrossRef]

134. Wang, J.; Zhang, Z.; Zhang, Y.N.; Han, D.; Medraj, M. Investigation on metallic glass formation in Mg-Zn-Sr ternary system by the CALPHAD method. *Mater. Lett.* **2019**, *256*, 126628. [CrossRef]
135. Wang, J.; Zhang, Z.; Li, S.; Meng, L.; Rao, W.F. Experimental investigation and thermodynamic modeling of the Mg-Cu-Ca ternary system. *Calphad* **2021**, *75*, 102325. [CrossRef]
136. Wang, J.; Chen, P.; Meng, L.; Jin, L. Investigation on the Mechanical and Corrosion Properties of ZnMnSr Alloys for Biodegradable Orthopedic Implants. *Adv. Eng. Mater.* **2022**, 2101581. [CrossRef]
137. Zhang, Z.; Zhang, Q.; Jin, L.; Zhang, Y.; Sheng, L. Experimental determination of the phase equilibrium in the Mg-Cu-Ca ternary system at 350 °C. *J. Alloys Compd.* **2019**, *818*, 152865. [CrossRef]
138. Wang, J.; Zhang, Z.; Jung, I.H.; Sheng, L. Experimental investigation and thermodynamic modeling of the Mg-Sn-Sr ternary system-ScienceDirect. *Calphad* **2021**, *72*, 102237. [CrossRef]
139. Wang, J.; Han, D.; Zhang, Z.; Jung, I.H.; Rao, W.F. Experimental measurement and thermodynamic evaluation of the Mg-Cu-Sr ternary system. *J. Chem. Thermodyn.* **2021**, *163*, 106582. [CrossRef]